The Composite Life Cycle of West Pacific Jet Superposition Events and their Associated Large-Scale Environments

Zachary J. Handlos*

Georgia Institute of Technology, Atlanta, Georgia

Jonathan E. Martin

University of Wisconsin–Madison, Madison, Wisconsin

**Corresponding author address:* Georgia Institute of Technology, 311 Ferst Drive, Atlanta, GA 30332-0340.

E-mail: zachary.handlos@eas.gatech.edu

ABSTRACT

Vertical alignment of the polar and subtropical jet streams in the west Pacific basin occurs most often in boreal winter. Recent work has revealed that the large-scale environments conducive to producing such superpositions involves interaction between East Asian Winter Monsoon (EAWM) cold surge events, lower latitude convection and internal jet dynamics. The evolution of the large-scale environments associated with these events post-superposition as well as the significance of that evolution on aspects of the wintertime Northern Hemisphere general circulation is examined. The post-superposition west Pacific jet extends eastward associated with an anomalous positive/negative PV couplet straddling the jet's exit region. This feature is shown to occur consistently amongst the majority of cases considered in the composite without regard for the seasonal strength of the EAWM. The positive/negative PV anomaly couplet, enhanced jet entrance circulation, low latitude convection and internal jet dynamics present in the pre-superposition environment weaken post-superposition. Discussion of the implications of jet extension on the large-scale circulation of the Northern Hemisphere as well as the predictability of west Pacific superposition events is undertaken.

1. Introduction

The genesis, evolution, and dissipation of extratropical weather systems and related mid-latitude phenomena are often linked to the evolution of the Northern Hemisphere polar (PJ) and subtropical jet streams (STJ), which have been researched extensively over the past several decades (e.g., Namias and Clapp 1949; Loewe and Radok 1950a,b; Yeh 1950; Koetswaram 1953; Mohri 1953; Koetswaram and Parthasarathy 1954; Newton 1954; Sutcliffe and Bannon 1954; Defant and Taba 1957; Krishnamurti 1961; Riehl 1962; Reiter 1963; Palmén and Newton 1969; Keyser and Shapiro 1986; Shapiro and Keyser 1990). The PJ resides above regions of strong baroclinicity within the middle latitudes (usually poleward of 30° latitude), and its speed maxima is observed $\sim$ 300 hPa. The PJ is also referred to as the "eddy-driven" jet, with several studies demonstrating that the PJ results from convergence of eddy momentum flux associated with developing waves in a region of enhanced mid-latitude baroclinicity (e.g., Held 1975; Rhines 1975; McWilliams and Chow 1981; Panetta 1993). The STJ resides primarily within the upper troposphere on the poleward edge of the Hadley Cell (Krishnamurti 1961), is associated with a weaker and shallower horizontal temperature gradient than the PJ and is primarily driven by angular momentum transport via convection in the equatorial latitudes.

Both the PJ and STJ reside in regions of strong gradients in tropopause height and potential vorticity. This is consistent with observations (e.g., Davies and Rossa 1998) as well as theory, which clearly relates strong gradients in quasi-geostrophic potential vorticity (QGPV) to local maxima in geostrophic wind speed (see Cunningham and Keyser 2004; Handlos and Martin 2016; Christenson et al. 2017, for a more detailed explanation). Defant and Taba (1957) were the first to note the relationship between the jets and a steep tropopause. They constructed maps of tropopause height in hPa (Fig. 1a) and noted the related regions of sharp gradient in such depictions were

observationally related to the two jets. The STJ resides between the "tropical" and "subtropical" tropopause steps while the PJ resides between the "subtropical" and "polar" tropopause steps. Such "steps" are clearly discernible in mean meridional cross-sections such as that shown in Fig. 1b.

Considerably less research attention has been given to instances of vertical superposition of the PJ and STJ, described as "vertical jet superpositions" by Winters and Martin (2014); Handlos and Martin (2016); Winters and Martin (2016); Christenson et al. (2017); Winters and Martin (2017). Vertical jet superposition results in a single jet core with wind speed maxima notably stronger than the separate polar and subtropical jets (Fig. 1c,d and Fig. 8 of Christenson et al. 2017). The leading structural characteristic of such features is the deep, nearly vertical tropopause "wall" separating the tropical and polar tropopause steps.

Among the handful of prior studies on this topic, Mohri (1953) performed a case study of a west Pacific vertical jet superposition event, which, to our knowledge, represents the only study of such an event observed in this region. Reiter (1961) and Reiter (1963) describe the possibility of PJ/STJ merger via vertical superposition of one jet stream upon the other. Reiter and Whitney (1969) investigate a superposed jet over the continental United States, stating that such merged jets do not seem to "behave" in the same manner as isolated PJ or STJ entities.

Recent research studies have revitalized interest in investigating vertical jet superpositions. For example, Christenson et al. (2017) constructed a Northern Hemisphere climatology of such events, finding that despite their rarity, the maximum frequency of occurrence of superpositions occurs during boreal winter (i.e., November, December, January, February and March) within the west Pacific (Fig. 2). Winters and Martin (2014, 2016) showed that a jet superposition was an integral component of the 2010 Nashville flood in the eastern United States as well as a mid-Atlantic blizzard in December 2009. Other extreme weather events have been found to be associated with ver-

tical jet superposition, including the late April 2011 southeastern United States tornado outbreak (Christenson and Martin 2012). Finally, cursory re-examination of the synoptic environments associated with previously studied extreme weather events suggests that some of these events may have been associated with a vertical jet superposition (Hoskins and Berrisford 1988; Shapiro and Keyser 1990; Hakim et al. 1996; Bosart et al. 1996). Thus, improving understanding of vertical jet superposition development and its relationship to extreme weather will enhance theoretical understanding of these events as well as the ability to forecast such events within the operational community.

Handlos and Martin (2016) composited 44 boreal winter west Pacific vertical jet superposition events and investigated the evolution of the large-scale environments conducive to PJ/STJ superposition. They found that several key large-scale features associated with the East Asian Winter Monsoon (EAWM) are tied to west Pacific vertical jet superposition events (Fig. 3). For example, a standardized anomalous positive geopotential height feature at 250 hPa is observed ($\phi_{250,std.anom}$) on the anticyclonic shear side of the composite jet (Fig. 3a). An anomalous trough feature at 500 hPa ($\phi_{500,std.anom.}$) with magnitude $< -1\sigma$ resides east of Japan (Fig. 3b). At 925 hPa, a negative standardized temperature anomaly ($T_{925,std.anom.}$) with anomalous northerly winds resides to the east and south of China (Fig. 3c), suggesting the occurrence of anomalous cold air advection there. This EAWM northerly cold surge propagates equatorward prior to jet superposition occurrence, strengthening anomalous convection present over the South China Sea and Malaysia (Fig. 3d). Outflow from this convection is advected towards the anticyclonic shear side of the west Pacific jet, forming a positive pressure depth anomaly within the isentropic layer housing the STJ that induces anomalous anticyclonic flow and strengthens the wind speed within the jet core. They showed that this, along with geostrophic cold air advection within the core of the jet entrance

region, characteristically leads to the development of the vertical PV "wall" characteristic of a vertical jet superposition.

While Handlos and Martin (2016) established a framework for understanding the precursor large-scale environments associated with jet superposition in the west Pacific (including understanding of the relationship between superposition events and the EAWM in this region), the subsequent life cycle of the superpositions and the evolution of their associated large-scale environments *after* superposition have not been investigated. Improving understanding of this post-superposition stage is beneficial for two reasons. First, such investigation will lead to a fuller understanding of the life cycle of robust vertical jet superposition events. Second, understanding the life cycle will provide insight regarding the influence the large-scale features associated with jet superposition exert on the general circulation of the Northern Hemisphere.

Motivated by the above, the goal of this study is to extend the analysis of Handlos and Martin (2016) in the context of understanding the spatial and temporal evolution of west Pacific jet superposition events and their environments after the time of superposition. Section 2 reviews the methodology to be used in this study. Section 3 discusses the evolution of the composite jet superposition after the two separate species are initially superposed. Section 4 investigates the evolution of the vertical jet structure within the composite jet superposition jet core and jet entrance regions. Section 5 explores the evolution of west Pacific jet superpositions in the context of the dominant modes of variability of the west Pacific jet stream. Section 6 concludes the study and suggests foci for future work.

2. Data and Methodology

As in Handlos and Martin (2016), NCEP/NCAR Reanalysis 1 data (Kalnay et al. 1996) is utilized for all variables and calculations involved in this study. The data have a 2.5° horizontal

grid spacing and 6-hourly temporal resolution. Data on both isobaric (unevenly spaced between 100-1000 hPa) and isentropic surfaces (interpolated every 5 K and examined in the 315-330 K and 340-355 K layers[1]) are used.

a. Identification of Robust West Pacific Jet Superposition Events

Table 1 shows the 44 robust west Pacific jet superposition cases identified in Handlos and Martin (2016) during the 31-winter period 1979/80-2009/10 (where boreal winter is defined as the months of December, January and February with leap days excluded). These superposition events were identified using a jet superposition identification (ID) scheme used by Christenson (2013), Winters and Martin (2014), Winters and Martin (2016), Handlos and Martin (2016), and Christenson et al. (2017). The scheme evaluates characteristics of the PV and wind speed distributions within each grid column over the Northern Hemisphere. Within the 315-330K (340-355K) layer, where the PJ (STJ) has been shown to reside during boreal winter (Christenson et al. 2017), whenever $|\nabla PV|$ within the 1-3 PVU channel exceeds or is equal to a threshold value[2] and the integral average wind speed in the 400-100 hPa layer $\geq 30\ m\ s^{-1}$, a polar (subtropical) jet is identified in that grid column. A vertical jet superposition event is identified if both the PJ and STJ criteria are met within the same grid column. For a date/time to be considered a "robust" event, 7 or more ID's are required to occur within a limited region of the west Pacific (defined as 30-40°N, 135-175°E) at a 6-hourly analysis time. We define the time of jet superposition occurrence, T=0, as the time at which the above criterion is met so long as the total number of ID's occurring 6 hours before (after) the identified 6-hourly time is less than (less than or equal to) the number of ID's observed at the time of superposition.

[1]The 315-330K and 340-355K layers were computed by averaging all levels between 315-330K and 340-355K, respectively.

[2]The threshold value is $0.64x10^{-5}\ PVU\ m^{-1}$ for both the 315-330K and 340-355K layers.

b. Composite Analysis

We utilize the composite analysis method of Handlos and Martin (2016) to investigate the temporal evolution of west Pacific superposition events and their associated large-scale features after T=0. We construct composite maps containing either anomalous or standardized anomalous quantities of interest as follows:

$$X_{std.anom.} = \frac{X_{supj} - X_{climo}}{X_{stdclimo}} \tag{1}$$

where $X_{std.anom.}$ is the standardized anomalous variable for a superposition event, X_{supj} is the variable measured at the point of interest at the time of interest, X_{climo} is the climatological value of the variable and $X_{stdclimo}$ is the standard deviation of the 31-winter climatology of variable X.

3. Composite Environments Associated with West Pacific Jet Superposition Events after Time of Superposition

Figures 4-7 consider the standardized anomalous quantities of interest from Fig. 3 with respect to composite robust west Pacific vertical jet superposition for 1-4 days after composite jet superposition occurrence, respectively. In these figures, only statistically significant values at the 95% confidence level based on a two-tailed student t-test are plotted[3]. At time T+1 (Fig. 4), the composite superposed jet has extended eastward and weakened to a maximum wind speed in the range of 80-90 m s^{-1}. Figure 4a shows a strengthening of the magnitude of the positive $\phi_{250,std.anom.}$ anomaly relative to the previous composite day (i.e., Fig. 3a), and this feature remains associated with strong anomalous anticyclonic flow. The anomalous negative ϕ on the cyclonic shear side of the composite jet remains about the same magnitude at 250 and 500 hPa (Figs. 4a and 4b). Figure

[3]With respect to anomalous wind, only vectors where both the zonal and meridional wind components exceed the 95% limit are shown.

4c shows that the anomalous cold air associated with anomalous northerly winds over the East and South China Seas still persists, though by this time the feature has started to shift eastward as the jet extends eastward. Anomalous negative OLR values remain anchored near Indonesia (Fig. 4d). However, with the eastward movement of the positive $\phi_{250,std.anom.}$ feature equatorward of the jet, the anomalous southwesterlies in the upper troposphere that were in a position to advect anomalous convective outflow away from the Maritime Continent region at time T=0 are now shifting away from the anomalous convection.

Throughout the rest of the Northern Hemisphere, there are only a few locations where any of the variables plotted exceed $\pm$ 0.5σ (or $\pm$ 10 W m^{-2} for anomalous OLR) and are statistically significant. One such region is northern Russia, where significant ϕ anomalies in the mid- to upper troposphere are observed. Another is over the Northwest Territories, where a warm anomaly in the lower troposphere meets the criteria. A $\sim$ 50 m s^{-1} composite jet resides over the east coast of the U.S., though the wind anomalies associated with this jet do not exceed 0.5σ (not shown). Thus, at time T+1, the majority of standardized anomalous large-scale elements exceeding the 0.5σ threshold are located near the west Pacific superposed jet.

At time T+2 (Fig. 5), the composite jet continues to extend eastward, maintaining about the same magnitude within its core. While the positive and negative $\phi_{250,std.anom.}$ and $\phi_{500,std.anom.}$ features remain relatively unchanged at this time (with a slight weakening of the negative ϕ anomaly at 500 hPa), these features reside within the right and left jet exit regions as the jet extends (Figs. 5a,b). The composite cold surge feature has now weakened substantially, with remnant anomalous northerly winds and cold air present northeast of Indonesia (Fig. 5c). Anomalous warm air associated with anomalous southerly winds south and east of the center of the upper tropospheric anomalous cyclonic circulation within the left jet exit region is observed south of Alaska. Centered along coastal British Columbia, anomalous positive ϕ in the middle to upper troposphere

indicates the presence of a composite anomalous ridge, though the flow itself near this anomaly does not exhibit statistical significance. Finally, the areal extent of anomalous convection in the Maritime Continent region, as well as the magnitude of the negative OLR anomalies, decreases (Fig. 5d). With the anomalous convection and its outflow dissociated from the upper tropospheric anomalous anticyclonic flow on the anticyclonic shear side of the jet, the convective flux of high θ_e, low-PV air is no longer a primary forcing supporting composite west Pacific jet superposition.

Revisiting other notable large-scale environments throughout the Northern Hemisphere, the magnitude of $\phi_{250,std.anom.}$ has fallen below the 0.5σ threshold over nearly all of northern Russia. The ϕ anomaly at 250 and 500 hPa over the Caspian Sea still remains, shifting slightly northeastward relative to the previous day (Figs. 5a and 5b). There is a small area where $T_{925,std.anom.} \geq 0.5\sigma$ in this region as well, and this threshold is also exceeded in extreme northern Russia and again within the Northwest Territories (Figs. 5c). Lastly, the jet over the western Atlantic has remained relatively stationary, weakening slightly.

At time T+3 (Fig. 6), the core of the composite jet continues to extend eastward. The anomalous ϕ features in the jet exit regions are still present in the 250 hPa and 500 hPa composites. The region of $\phi_{250,std.anom.} > 0.5\sigma$ over the Northwest Territories expands in areal extent (Fig. 6a) though weakens slightly at 500 hPa (Fig. 6b). Figure 6c shows the remnants of the anomalous cold surge propagating eastward, with the area of cold air $\leq$ -0.5σ continuing to decrease. A warm air anomaly associated with the ridge over Alaska still persists, while the warm air anomaly region southeast of the west Pacific jet core shrinks in size. The region of negative OLR values near Indonesia continues to shrink as well (Fig. 6d). Outside of the continued presence of a ϕ anomaly just east of the Caspian Sea and features near Alaska, the rest of the Northern Hemisphere is free of composite features of interest by this time.

Finally, 4 days after composite west Pacific vertical jet superposition (Fig. 7), the majority of the large-scale elements referenced earlier have dissipated. For example, the maximum wind speed associated with the composite jet decreases, though the jet does continue to extend farther eastward. The ϕ anomalies at 250 and 500 hPa remain comparably vigorous while shifting slightly eastward with the extension of the jet (Figs. 7a and 7b). The composite standardized anomalous temperature $< 0.5\sigma$ has nearly disappeared (Fig. 7c) as has the warm air feature in the jet exit region. The lower tropospheric warm air anomaly first noted at time T+2 over eastern Alaska is still present over eastern Alaska and northwestern Canada at this time. Along with the dissipation of the cold and warm air anomalies observed in the jet exit region, both the areal extent and magnitude of negative OLR near Indonesia continue to decrease (Fig. 7d). The Caspian Sea ϕ anomaly in the mid- to upper troposphere has also nearly disappeared by this time.

In summary, Figs. 4-7 illustrate that the following elements characterize the large-scale environment throughout this 4-day period: 1) an eastward extension of the west Pacific jet, 2) the continued presence of the mid- to upper tropospheric positive and negative ϕ anomalies, particularly within the right and left jet exit regions, respectively, 3) the dissipation of the anomalous cold surge event as it propagates eastward across the Pacific Ocean, 4) a progressive disconnect between the anomalous convection and west Pacific jet, and 5) the absence of any statistically significant features of interest outside of the Pacific basin other than the anomalous positive ϕ features in northern Russia and near the Caspian Sea. The next subsection quantifies the fraction of individual cases within the composite that exhibit these key features.

a. Frequency of Occurrence of Key Large-Scale Environmental Features and their Coherence Post-Jet Superposition

In order to determine whether the observed standardized anomalous features in the 44-case composite occurred within the majority of cases examined, Handlos and Martin (2016) considered the percent occurrence of cases for each grid point in which the $\pm$ 0.5σ threshold was exceeded for several standardized anomalous variables of interest. This same analysis is repeated for times T+1 through T+4 to determine if the large-scale environments that characterize the composite evolution post-superposition occur within the majority of the 44 cases.

Figures 8-11 show plots of the frequency of occurrence of grid points $\geq \pm$ 0.5σ out of the 44 total vertical jet superposition events used in our composite analysis at times shown in Figs. 4-7. With respect to $\vec{u}_{250,std.anom.}$, as many as $>$ 90% of cases fulfill this requirement within the west Pacific jet core at time T+1 (Fig. 8a). A similarly large fraction ($\geq$ 70-80%) of cases exhibit grid points $\leq$ -0.5σ in regions flanking the jet core meridionally. Throughout the evolution of the extension of the composite jet (Figs. 9a, 10a and 11a), the frequency of occurrence for all wind anomalies associated with the extended, narrow jet remains $\geq$ 60-80%. Within the western portion of the jet, the percent occurrence decreases throughout the extension. Thus, while the eastward extension of the jet occurs within the majority of cases included in the composite, significant jet variability exists upstream.

Panel b in Figs. 8-11 show that the $\phi_{250,std.anom.}$ feature on the anticyclonic shear side of the composite jet occurs in $\geq$ 90% of cases or more in some grid points as this anomaly moves eastward over time. Interestingly, the number of events where the negative standardized anomalous threshold is met at 250 hPa in the composite left jet exit region increases between T+1 and T+2 (Figs. 8b and 9b), remaining relatively constant even up to time T+4 (Figs. 10b and 11b). Thus,

the persistence of the anomalous ϕ features within the jet exit region characterizes the majority of cases comprising the composite.

The findings above are also observed at 500 hPa (panel c in Figs. 8-11). The number of cases where $\phi_{500,std.anom.} \leq$ -0.5σ on the cyclonic shear side of the jet (associated with the anomalous trough-like feature) is as high as $\geq$ 90% of cases at time T+1 (Fig. 8c), with the maximum percent of cases in the core of this anomaly remaining somewhere between $\geq$ 70-80% through time T+4. The anomalous positive ϕ feature equatorward of the jet at 500 hPa exceeds the 0.5σ threshold in more cases at time T+4 than time T+1 (Figs. 8c vs. 11c).

Finally, with respect to the eastward propagation and dissipation of the anomalous cold surge feature, the number of cases exhibiting anomalous cold air exceeding the 0.5σ threshold decreases consistently over the 4 days (panel d of Figs. 8-11). On the other hand, over 50-70% of cases are associated with the development of the warm air anomaly near Alaska throughout the 4-day period. This coincides with a weak signature (based on this metric) of consistent anomalous positive ϕ in the mid- to upper troposphere, where the highest percent occurrence over the Northwest Territories exceeds 60% of cases at times T+2 and T+3 (Figs. 9b,c and 10b,c). Therefore, many of the robust superposition cases exhibit anomalous ridging and warming in this region within a few days after superposition.

Recall that regions of anomalous positive ϕ at 250 hPa and 500 hPa were identified over the Caspian Sea and northern Russia. These features occur within $>$ 50% of cases at times T+1, T+2 and T+3 (panels b and c of Figs. 8-10). At time T+4, the percent occurrence of anomalous ϕ over northern Russia dissipates, and the percent occurrence maximum over the Caspian Sea shifts northeastward. While there are some other regions of the hemisphere that exhibit grid points exceeding 50% for $\vec{u}_{250,std.anom.}$, $\phi_{250,std.anom.}$, $\phi_{500,std.anom.}$ and $T_{925,std.anom.}$, these regions are not associated with any features of interest from the composites of Figs. 4-7.

To summarize, Figs. 8-11 show that the the occurrence of an extended jet, anomalous ϕ maximum and minimum features within the composite jet exit regions at 250 hPa and 500 hPa, dissipation of the northerly cold surge anomaly and anomalous warm air and ridging in Alaska at 925 hPa occur within the majority of the cases included in the composite. The evolution of these features is consistent up to 4 days after superposition occurrence. Thus, results suggest that these features are associated with the evolution of the west Pacific jet post-superposition within the majority of cases considered within the composite analysis.

4. Post-Superposition Evolution - Composite Cross Section Perspective

Handlos and Martin (2016) showed that the vertical structure of the composite west Pacific jet, when superposed, exhibited the characteristic two-step tropopause structure with a deep, vertical PV wall within the jet core. This PV wall was a function of high-θ_e, low-PV air from lower latitude convection manifesting itself within the STJ isentropic layer equatorward of the jet core, while high-PV air associated with subsidence forced by geostrophic cold air advection in cyclonic shear within the jet entrance region induced a positive PV anomaly poleward of the jet core (see their Fig. 17). Coincidentally, the authors observed an anomalously strong jet entrance region circulation at the time of jet superposition occurrence. In this section, composite cross sections through the jet core and jet entrance regions are again considered but in the context of the post-superposition evolution of the vertical structure of the composite jet.

Figures 12 and 13 show cross-sections taken through the west Pacific jet core at times T+1 through T+4 (see Figs. 4a-7a for cross-sectional slices A-A'). Over the 96 hour period after composite vertical jet superposition occurrence, the characteristic vertical PV wall observed at time T=0 (Fig. 7 from Handlos and Martin 2016) exhibits a less vertical orientation. Associated with

this, the magnitude of the positive and negative Ertel PV anomalies on the poleward and equatorward sides of the jet core weaken.

The eastward propagation of the anomalous anticyclonic flow that previously advected high-θ_e, low-PV air towards the anticyclonic shear side of the jet core is no longer prevalent post-superposition (recall Figs. 4d-7d). This, along with the eastward propagation of the positive $\phi_{250,std.anom.}$ anomaly equatorward of the jet into the right jet exit region explains the weakening of the negative PV anomaly associated with the composite jet core. The weakening of the positive PV anomaly is tied to the eastward propagation into the left jet exit region of the anomalous mid-tropospheric $\phi_{250,std.anom.}$ feature. As a result of the above, the vertical tropopause structure evolves towards a state that is structurally similar to the climatological two-step tropopause of the west Pacific jet, exhibiting a less steep vertical tropopause wall and a weaker wind speed (Fig. 7a in Handlos and Martin 2016).

Figure 14 shows cross-sections taken through the west Pacific jet entrance region at times T+1 through T+4, highlighting anomalous vertical motion. The cross section at time T+1 (Fig. 14a) reveals an anomalously strong and equatorward shifted thermally direct circulation similar to that observed at the time of jet superposition (Fig. 8 of Handlos and Martin 2016). However, this anomalous circulation is weaker than at time T=0. This circulation continues to weaken at times T+2 through T+4 (Figs. 14b-d).

Handlos and Martin (2016) showed that the enhanced and equatorward-shifted jet entrance region circulation was tied to geostrophic cold air advection within the core of the jet entrance region of the composite jet. The induced subsidence within the jet entrance region "draws" high-PV air from the lower stratosphere downward, increasing the magnitude of anomalous positive PV (e.g., Eliassen 1962; Shapiro 1982; Keyser and Pecnick 1985; Martin 2014). At times T+1 through T+4 (Fig. 15), a decrease in the magnitude of geostrophic cold air advection within the entrance region

is observed. This is associated with a decrease in the magnitude of subsidence, implying a reduction in the downward protrusion of high-PV stratospheric air. This, in concert with the eastward propagation of the mid-tropospheric anomalous trough, leads to the demise of the positive PV anomaly poleward of the jet core.

The cross-sections through the 44-case composite west Pacific jet core and entrance regions post-superposition reveal the following: i) A less vertically oriented PV wall associated with a weakening of both positive and negative PV anomalies flanking the jet core and ii) a weakening of the anomalous thermally direct circulation associated with the composite jet entrance region. The weakening of the composite vertical jet superposition structure is tied to the eastward propagation of both negative and positive geopotential height anomaly features, which become embedded within the jet exit regions, the lack of anomalous anticyclonic flow present equatorward of the jet to advect high-θ_e, low-PV air towards the jet core and the weakening of geostrophic cold air advection in the core of the jet entrance region. These findings show that these features and processes are all necessary for both the development and sustenance of a jet superposition event.

5. Jet Superposition Extension and Poleward Extent and Relationship to the Large-Scale Circulation

The extension (or retraction) of the west Pacific jet has been shown to be associated with several teleconnection phenomena. This includes (but is not limited to) the Pacific-North American (PNA) pattern, extreme precipitation events in the Pacific including the western U.S., Kona Low events near Hawai'i, significant ridge building events near Alaska and the Madden-Julian Oscillation (e.g., Chu et al. 1993; Otkin and Martin 2004; Jaffe et al. 2011; Griffin and Martin 2017). Given that the composite results reveal an extension of the west Pacific jet stream regardless of EAWM strength, and given the connection the jet has with weather and climate within the North-

ern Hemisphere, it is of interest to determine if any relationship exists between metrics used to determine the extension/retraction "mode" of the west Pacific jet with that of the results from the composite analysis. Such metrics could prove beneficial in tracking the evolution of west Pacific jet superposition events and associated changes to the large-scale Northern Hemisphere circulation.

To quantify the magnitude and evolution of the zonal extension/retraction and meridional shift of west Pacific vertical jet superposition events, we adapt the methodology of Jaffe et al. (2011) and extract the two leading modes of Pacific jet variability by performing a principal component analysis (PCA) on 300 hPa zonal wind over the basin (i.e., 20-80°N, 100°E-60°W). Note that this analysis employs daily average data, includes the months of November and March, and applies a 5-day running mean to filter out high frequency variability to be consistent with that of Jaffe et al. (2011). The two most dominant modes of jet variability are the following: 1) The zonal extension/retraction of the exit region of the west Pacific jet across the Pacific Ocean and 2) the poleward/equatorward shift of the jet over the west- and central Pacific (not shown). Since we are interested in the time evolution of these two modes of variability, we consider the principal components (PC's) of each mode.

Figure 16a shows a phase space diagram of principal components 1 and 2 (PC1 and PC2, respectively) with respect to the composite superposition evolution (i.e., green solid line), constructed by averaging the PC1 and PC2 values for all 44 cases at each time step and plotting the temporal evolution of the composite values. In this figure, the evolution of both PC1 and PC2 modes from time T-5 days to T+5 days is shown. We observe an increase in the magnitude of PC1 from T-5 days through T+3 days. This indicates an extension of the west Pacific jet over this timeframe, which is consistent with the time evolution of the composite jet shown in this study. Between times T+3 and T+5, PC1 remains about the same value and then decreases slightly while the magnitude of

PC2 increases. This implies a slight retraction of the jet as well as a poleward shift. While we only show plots at times T+3 and T+4 (Figs. 6-7), the continued extension of the jet is not exhibited at time T+4, however the exit region of the jet does appear to shift poleward slightly during this time. These observations are consistent with the jet variability PCA-metric, suggesting that PC modes 1 and 2 (Fig. 16a) accurately represent the structural evolution of the composite west Pacific jet prior to, during and after superposition.

Nonetheless, significant variability exists with respect to west Pacific jet extension/retraction and poleward/equatorward shift evolution when considering each of the 44 jet superposition cases individually. This is demonstrated by the variability in the location of starting, middle and ending points (i.e., PC1/PC2 values at T-5, T=0 and T+5, respectively), of the PC1/PC2 evolution for all cases (Figs. 19b-d). At T-5 days (Fig. 16b), the number of superposition cases that fall within the "retracted/poleward shifted" (top-left; PC1 $<$ 0 and PC2 $>$ 0), "extended/poleward shifted" (top-right; PC1 $>$ 0 and PC2 $>$ 0) and "extended/equatorward shifted" (bottom-right; PC1 $>$ 0 and PC2 $<$ 0) quadrants are similar; only 5 cases fall within the "retracted/equatorward shifted" (bottom-left; PC1 $<$ 0 and PC2 $<$ 0) quadrant at this time. At T=0 (Fig. 16c), although variability in PC1/PC2 value is still evident, the cases appear to be converging towards the "jet extension/poleward shift" (i.e., upper-right) quadrant. By T+5 days (Fig. 16d), the majority of cases reside within the "extended/poleward shifted" quadrant (i.e., 26 of 44 cases). At this time, 34 of 44 cases exhibit PC1 $>$ 0, indicating an extended jet, and 34 of 44 cases exhibit PC2 $>$ 0. Given this and our composite results from a plan view perspective, the large-scale environments associated with the west Pacific jet post-superposition are biased towards encompassing the extension of the jet across the Pacific Ocean as well as a redirection toward the pole.

Jaffe et al. (2011) (e.g., their Figure 9b) and Griffin and Martin (2017) (e.g., their Figure 4c), investigating west Pacific jet PC modes 1 and 2 via EOF and time-extended EOF analysis, re-

spectively, showed that anomalous cyclonic and anticyclonic flow resides within the left and right exit regions of the jet during west Pacific jet extension. Both studies also demonstrate ridge-building near Alaska during west Pacific jet extension. These findings are consistent with our post-superposition composite results without regard for EAWM strength.

Furthermore, Griffin and Martin (2017) show that anomalous cold air is present 5 days prior to maximum jet extension occurrence, and anomalous convection is present within the Maritime Continent at times T-5, T=0 and T+5 relative to maximum poleward shift of the jet. This suggests that cold surge events and associated anomalous convection at lower latitudes serve as precursor events associated with subsequent west Pacific jet extension/poleward shift. In summary, the results from this study in concert with findings from Jaffe et al. (2011), Handlos and Martin (2016) and Griffin and Martin (2017) show that the identification of a jet superposition event and associated EAWM cold surges may serve as tools for predicting west Pacific jet extension and poleward shift and the evolution of the Northern Hemsiphere large-scale circulation on synoptic timescales (i.e., $\sim$ 5 days). PC's 1 and 2 can be used in concert with the above observations to aid in tracking the evolution of the above phenomena.

6. Conclusions

The goal of this study was to explore the evolution of west Pacific vertical jet superposition events and their associated large-scale environments in the days following initial superposition. The same composite and case-study analysis techniques used in Handlos and Martin (2016) were applied but at times T+n relative to superposition (n $>$ 0 days). These evolutions were investigated within the context of the 44-case, strong and neutral EAWM season composites.

Figure 17 highlights the key large-scale phenomena observed at the time of jet superposition (Fig. 17a; adopted from Fig. 17 of Handlos and Martin 2016) and after time of jet superposition

within the 44-case composite (Fig. 17b). West Pacific jet superposition events are commonly associated with an EAWM northerly cold surge event that propagates equatorward and enhances convection via enhanced surface convergence (dark blue oval with purple arrows interacting with cloud symbols in Fig. 17a). Convective outflow (green stippled arrow) is then advected toward the anticyclonic shear side of the jet, increasing anomalous vertical wind shear such that the magnitude of wind within the jet core increases. This convection, in concert with internal jet dynamics, also acts to develop the deep, vertical PV wall characteristic of west Pacific jet superposition events.

In general, and regardless of EAWM seasonal strength, the evolution of the composite environments are all associated with the following: 1) the extension of the west Pacific jet stream, 2) the maintenance of anomalous cyclonic (anticyclonic) flow in the left (right) jet exit region that migrates eastward as the jet extends, 3) ridging downstream of the extended jet, which can lead to trough/ridge development downstream over eastern North America and the North Atlantic, 4) weakening of the EAWM northerly cold surge, and 5) the propagation of upper tropospheric anomalous southwesterly flow away from anomalous convection observed over the Maritime Continent region. Throughout this evolution, the west Pacific jet is displaced increasingly eastward from the environments that led to superposition onset, perturbing the large-scale flow downstream and ultimately impacting the large-scale circulation throughout the Northern Hemisphere. Lastly, the composite large-scale evolutions described above are observed regardless of the strength of the EAWM (not shown), suggesting that EAWM seasonal strength exerts little influence on this observed composite life-cycle.

Examination of composite vertical cross sections through the composite jet core and entrance regions reveal the following: 1) weakening of the composite deep and vertical PV wall within the jet core, which is tied to the eastward propagation of the positive and negative PV anomalies (i.e., negative and positive geopotential height anomalies, respectively) flanking the jet core eastward

within the jet exit regions, and 2) a weakening of the thermally direct circulation within the composite jet entrance region. The second item is associated with the weakening of geostrophic cold air advection within the composite jet entrance region.

The evolution of the composite life-cycle of the west Pacific jet from time T-5 to time T+5 is well represented well using the two leading modes of jet variability extracted via PCA of 300 hPa zonal wind over the western Pacific. Despite significant variability in PC1/PC2 evolution characterizing each of the 44 cases individually, the cases exhibit an aggregate shift towards an extended/poleward shifted jet. Furthermore, the presence of northerly cold surge events along with anomalous low latitude convection prior to west Pacific jet superposition extension is consistent with the analysis of Griffin and Martin (2017). Thus, PC modes 1 and 2 may serve as a useful forecasting tool in tracking the evolution of jet extension and poleward shift events post-superposition in the west Pacific.

With recent research showing that extreme weather events can be influenced by jet superposition (Christenson and Martin 2012; Winters and Martin 2014, 2016), it is reasonable to consider the effect of west Pacific vertical jet superposition events on extreme weather over the Northern Hemisphere. This includes consideration of the relationship between tropical cyclones and west Pacific jet superposition, the development of significant extratropical cyclone events within the left exit region of these superposed jets and also their relationship to atmospheric blocking. The latter is especially of interest given the observed development of an anomalous ridge over western North America post-superposition. Exploration of these topic is also underway via case-study analysis of several events.

Lastly, to the authors' knowledge, this study, along with that of Handlos and Martin (2016), are the only studies that have investigated the evolution of the life-cycle of jet superposition events and their associated large-scale environments from a composite perspective. A similar study could

be readily performed using this same technique for other regions characterized by local maxima in frequency of occurrence of superposition events. For example, Christenson et al. (2017) show that these events occur frequently (relative to other regions of the Northern Hemisphere) in the southern U.S. as well as North Africa. The composite analysis of superposition events over such regions in order to compare and contrast the large-scale environments associated with superposed jet events in these regions with that of the west Pacific should be considered in the future. Results from such work would provide additional insight regarding variability in the genesis and lysis of jet superposition events.

Acknowledgments. This work is funded by the National Science Foundation through grant AGS-1265182.

References

Bosart, L. F., G. J. Hakim, K. R. Tyle, M. A. Bedrick, W. E. Bracken, M. J. Dickinson, and D. M. Schultz, 1996: Large-Scale Antecedent Conditions Associated with the 12-14 March 1993 Cyclone ("Superstorm '93") over Eastern North America. *Mon. Wea. Rev.*, **124**, 1865–1891.

Christenson, C. E., 2013: A Synoptic-Climatology of Northern Hemisphere Polar and Subtropical Jet Superposition Events. M.S. thesis, Department of Atmospheric and Oceanic Sciences, University of Wisconsin - Madison, 62 pp.

Christenson, C. E., and J. E. Martin, 2012: The Large-Scale Environment Associated with the 25-28 April 2011 Severe Weather Outbreak. In 16th Annual Severe Storms and Doppler Radar Conference, 31 March 2012. Des Moines, IA, National Weather Association: Norman, OK.

Christenson, C. E., J. E. Martin, and Z. J. Handlos, 2017: A Synoptic Climatology of Northern Hemisphere, Cold Season Polar and Subtropical Jet Superposition Events. *J. Climate*, **30**, 7231–7246.

Chu, P. S., A. J. Nash, and F. Y. Porter, 1993: Diagnostic Studies of Two Contrasting Rainfall Episodes in Hawaii: Dry 1981 and Wet 1982. *J. Climate*, **6**, 1457–1462.

Cunningham, P., and D. Keyser, 2004: Dynamics of Jet Streaks in a Stratified Quasi-Geostrophic Atmosphere: Steady-State Representations. *Quart. J. Roy. Meteor. Soc.*, **130**, 1579–1609.

Davies, H., and A. Rossa, 1998: PV Frontogenesis and Upper Tropospheric Fronts. *Mon. Wea. Rev.*, **126**, 1528–1539.

Defant, F., and H. Taba, 1957: The Threefold Structure of the Atmosphere and the Characteristics of the Tropopause. *Tellus*, **9**, 259–275.

Eliassen, A., 1962: On the Vertical Circulation in Frontal Zones. *Geophys. Publ.*, **24**, 147–160.

Griffin, K. S., and J. E. Martin, 2017: Synoptic Features Associated with Temporally Coherent Modes of Variability of the North Pacific Jet Stream. *J. Climate*, **30**, 39–54.

Hakim, G. J., D. Keyser, and L. F. Bosart, 1996: The Ohio Valley Wave Merger Cyclogenesis Event of 25-26 January 1978. Part II: Diagnosis using Quasigeostrophic Potential Vorticity Inversion. *Mon. Wea. Rev.*, **124**, 2176–2205.

Handlos, Z. J., and J. E. Martin, 2016: Composite Analysis of Large-Scale Environments Conducive to West Pacific Polar/Subtropical Jet Superposition. *J. Climate*, **29**, 7145–7165.

Held, I., 1975: Momentum Transport by Quasi-Geostrophic Eddies. *J. Atmos. Sci.*, **32**, 1494–1497.

Hoskins, B. J., and P. Berrisford, 1988: A Potential Vorticity Perspective of the Storm of 15-16 October 1987. *Weather*, **43**, 122–129.

Jaffe, S. C., J. E. Martin, D. J. Vimont, and D. J. Lorenz, 2011: A Synoptic-Climatology of Episodic, Sub-Seasonal Retractions of the Pacific Jet. *J. Climate*, **24**, 2846–2860.

Kalnay, E., and Coauthors, 1996: The NCEP/NCAR 40-Year Reanalysis Project. *Bull. Amer. Meteor. Soc.*, **77**, 437–471.

Keyser, D., and M. J. Pecnick, 1985: A Two-Dimensional Primitive Equation Model of Frontogenesis forced by Confluence and Horizontal Shear. *J. Atmos. Sci.*, **42**, 1259–1282.

Keyser, D., and M. A. Shapiro, 1986: A Review of the Structure and Dynamics of Upper-Level Frontal Zones. *Mon. Wea. Rev.*, **114**, 452–499.

Koetswaram, P., 1953: An Analysis of the High Tropospheric Wind Circulation over India in Winter. *Indian J. Meteor. Geophys.*, **4**, 13–21.

Koetswaram, P., and S. Parthasarathy, 1954: The Mean Jet Stream over India in the Pre-Monsoon and Post-Monsoon Seasons and Vertical Motions associated with Subtropical Jet Streams. *Indian J. Meteor. Geophys.*, **5**, 138–156.

Krishnamurti, T. N., 1961: On the Role of the Subtropical Jet Stream of Winter in the Atmospheric General Circulation. *J. Meteor*, **18**, 657–670.

Loewe, F., and V. Radok, 1950a: A Meridional Aerological Cross Section in the Southwest Pacific. *J. Meteor*, **7**, 58–65.

Loewe, F., and V. Radok, 1950b: Some Amendments to “A Meridional Aerological Cross-Section in the Southwest Pacific. *J. Meteor*, **7**, 305–306.

Martin, J. E., 2014: Quasi-Geostrophic Diagnosis of the Influence of Vorticity Advection on the Development of Upper Level Jet-Front Systems. *Quart. J. Roy. Meteor. Soc.*, **140**, 2658–2671.

McWilliams, J., and J. Chow, 1981: Equilibrium Geostrophic Turbulence I: A Reference Solution in a β-plane Channel. *J. Phys. Oceanogr.*, **11**, 921–949.

Mohri, K., 1953: On the Fields of Wind and Temperature over Japan and Adjacent Waters during Winter of 1950–1951. *Tellus*, **5**, 340–358.

Namias, J., and P. F. Clapp, 1949: Confluence theory of the high tropospheric jet stream. *J. Meteor*, **6**, 330–336.

Newton, C. W., 1954: Frontogenesis and Frontolysis as a Three-Dimensional Process. *J. Meteor.*, **11**, 449–461.

Otkin, J. A., and J. E. Martin, 2004: The Large-Scale Modulation of Subtropical Cyclogenesis in the Central and Eastern Pacific Ocean. *Mon. Wea. Rev.*, **132**, 1813–1828.

Palmén, E., and C. W. Newton, 1969: *Atmospheric Circulation Systems: Their Structure and Physical Interpretation.* Academic Press, 603 pp.

Panetta, R., 1993: Zonal Jets in Wide Baroclinically Unstable Regions: Persistence and Scale Selection. *J. Atmos. Sci.*, **50**, 2073–2106.

Reiter, E. R., 1961: *Meteorologie der Strahlströme (Meteorology of the Jet Streams)*. Springer-Verlag, Vienna, 473 pp.

Reiter, E. R., 1963: *Jet Stream Meteorology*. University of Chicago Press, 515 pp.

Reiter, E. R., and L. F. Whitney, 1969: Interaction between Subtropical and Polar-Front Jet Stream. *Mon. Wea. Rev.*, **97**, 432–438.

Rhines, P., 1975: Waves and Turbulence on a β-plane. *J. Fluid Mech.*, **69**, 471–443.

Riehl, H., 1962: Jet Streams of the Atmosphere. Tech. rep., Dept. of Atmospheric Science, Colorado State University Tech. Rep. 32, Fort Collins, Colorado, 117 pp.

Shapiro, M. A., 1982: Mesoscale Weather Systems of the Central United States. Tech. rep., CIRES Univ. of Colorado/NOAA: Boulder, CO, 78 pp.

Shapiro, M. A., and D. Keyser, 1990: Fronts, Jet Streams, and the Tropopause. *Extratropical Cyclones: The Erik Palmn Memorial Volume*, C. Newton, and E. O. Holopainen, Eds., Amer. Meteor. Soc., 167–191.

Sutcliffe, R. C., and J. K. Bannon, 1954: Seasonal Changes in the Upper-Air Conditions in the Mediterranean Middle East Area. *Scientific Proceedings of the International Association of Meteorology*, Rome, Italy, Int. Union of Geodesy and Geophysics, 322–334.

Winters, A. C., and J. E. Martin, 2014: The Role of a Polar/Subtropical Jet Superposition in the May 2010 Nashville Flood. *Wea. Forecasting*, **29**, 954–974.

Winters, A. C., and J. E. Martin, 2016: Synoptic and Mesoscale Processes Supporting Vertical Superposition of the Polar and Subtropical Jets in Two Contrasting Cases. *Quart. J. Roy. Meteor. Soc.*, **142**, 1133–1149.

Winters, A. C., and J. E. Martin, 2017: Diagnosis of a North American Polar/Subtropical Jet Superposition Employing Potential Vorticity Inversion. *Mon. Wea. Rev.*, **145**, 1853–1873.

Yeh, T. C., 1950: The Circulation of the High Troposphere over China in the Winter of 1945-46. *Tellus*, **2**, 173–183.

LIST OF TABLES

TABLE 1. List of 44 robust west Pacific vertical jet superposition events identified using the methodology described in Section 2.

Robust Event Date/Time	Robust Event Date/Time
07 February 1980 (0000 UTC)	14 February 1999 (1200 UTC)
29 December 1980 (0600 UTC)	23 December 1999 (0000 UTC)
11 January 1981 (0600 UTC)	31 January 2000 (0600 UTC)
29 January 1981 (1200 UTC)	16 February 2000 (1200 UTC)
14 December 1981 (1800 UTC)	17 February 2000 (0000 UTC)
15 December 1981 (1800 UTC)	11 December 2000 (0600 UTC)
04 February 1987 (0600 UTC)	04 January 2001 (0000 UTC)
10 January 1988 (0000 UTC)	04 January 2001 (1200 UTC)
23 February 1991 (1200 UTC)	15 January 2001 (0000 UTC)
24 February 1991 (1800 UTC)	15 January 2001 (1200 UTC)
25 February 1991 (1200 UTC)	16 January 2001 (0000 UTC)
24 February 1993 (1800 UTC)	19 February 2002 (1800 UTC)
25 December 1995 (0000 UTC)	21 December 2003 (0000 UTC)
25 December 1995 (1800 UTC)	26 December 2003 (1800 UTC)
01 February 1996 (0000 UTC)	07 February 2004 (0600 UTC)
02 February 1996 (1200 UTC)	27 December 2005 (1800 UTC)
01 December 1996 (0000 UTC)	10 January 2007 (0000 UTC)
01 December 1996 (1200 UTC)	15 February 2008 (0000 UTC)
02 December 1996 (0000 UTC)	16 February 2008 (0000 UTC)
09 January 1999 (1200 UTC)	16 February 2008 (1800 UTC)
12 January 1999 (1200 UTC)	08 January 2010 (1200 UTC)
13 February 1999 (0000 UTC)	15 January 2010 (1200 UTC)

LIST OF FIGURES

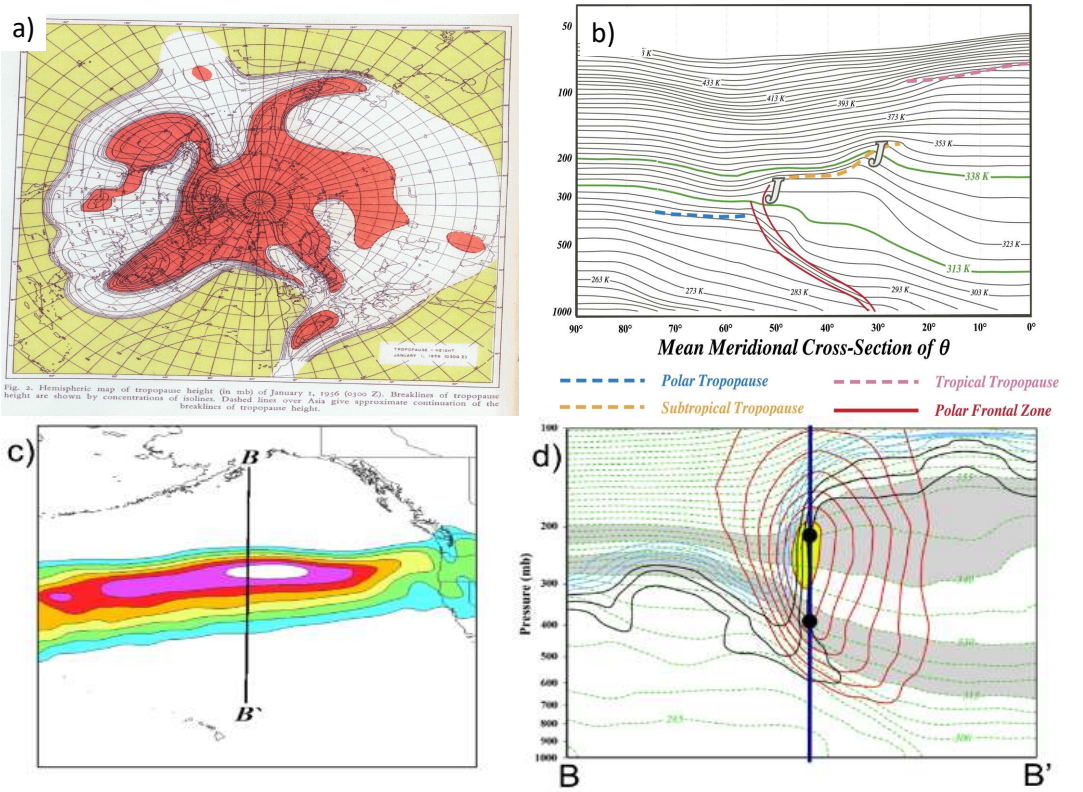

FIG. 1. a) From Winters and Martin (2014), color-enhanced (from DT57) mean meridional cross section of isentropic (θ) surfaces (units K, solid black lines) along with labeled jet stream locations ("J" symbols) and the tropical, subtropical and polar tropopause steps (dashed contours, see legend at bottom of figure) on 1 January 1956. The polar frontal zone is also labeled (solid red contour). b) From DT57: Tropopause height (hPa) over the Northern Hemisphere at 0300 UTC on 1 January 1956. The yellow regions represent the tropical tropopause height, white regions represent the subtropical tropopause height and red regions represent the polar tropopause height. The PJ (STJ) approximately resides along the strong concentrations in isolines bordering between the red and white (yellow and white) regions.

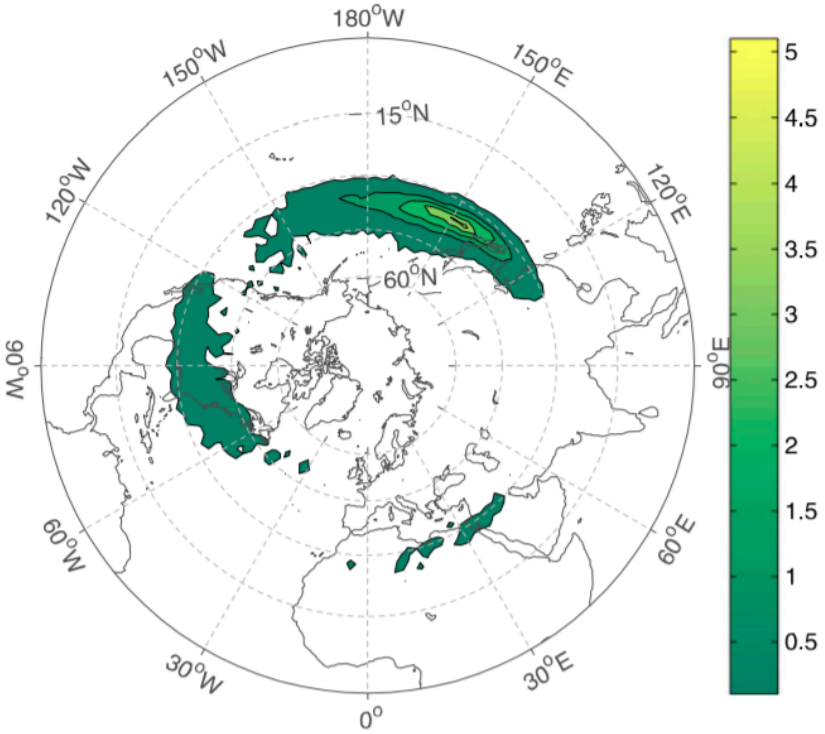

FIG. 2. Adopted from Christenson et al. (2017): Frequency of occurrence of vertical jet superposition events over the Northern Hemisphere during boreal winter months NDJFM 1960/61 - 2009/10.

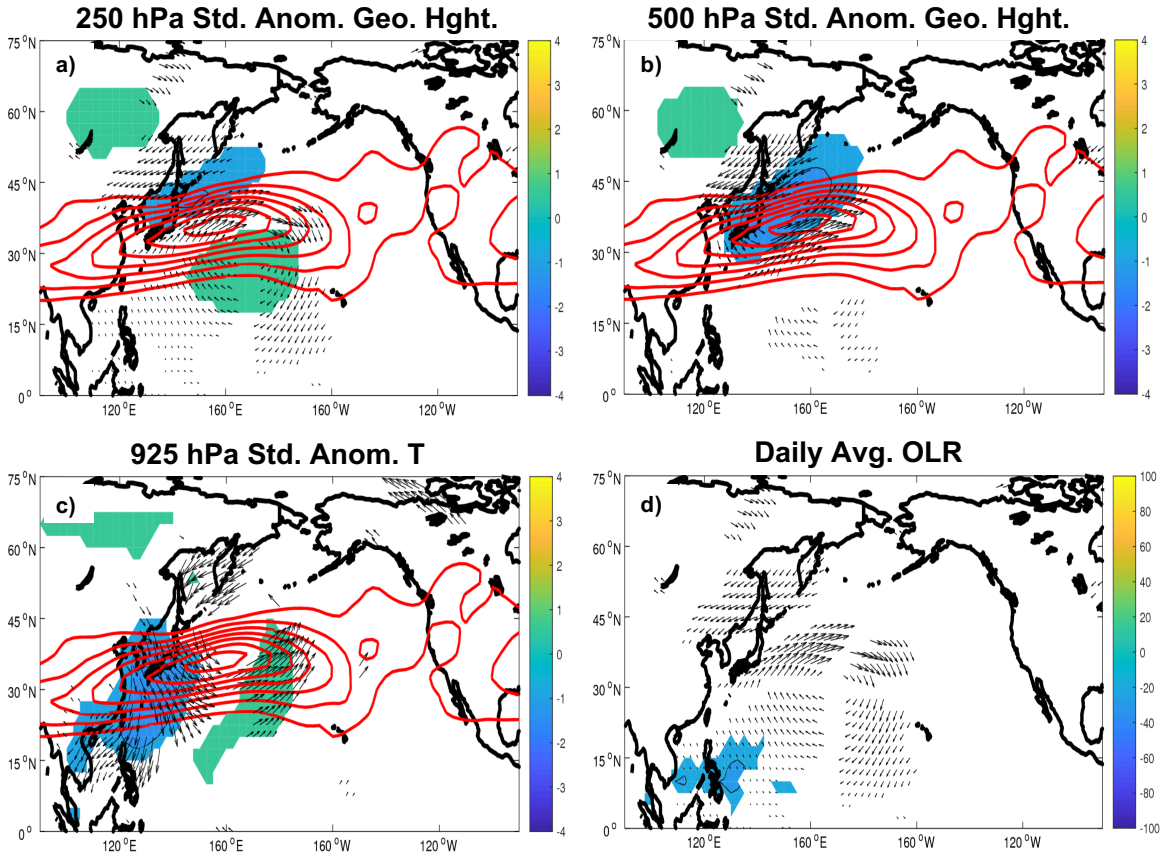

FIG. 3. Adopted from Handlos and Martin (2016), composite large-scale features at the time of composite west Pacific vertical jet superposition (i.e., time T=0). Shaded regions show positive (negative) standardized anomalous a) ϕ_{250}, b) ϕ_{500}, c) T_{925} and d) daily-averaged anomalous (non-standardized) OLR. Anomalous (non-standardized) winds are shown as black vectors. The red contour represents 250 hPa composite isotachs every 10 m s^{-1} starting at 30 m s^{-1}. Only anomalous values exceeding the 95% confidence limit are plotted.

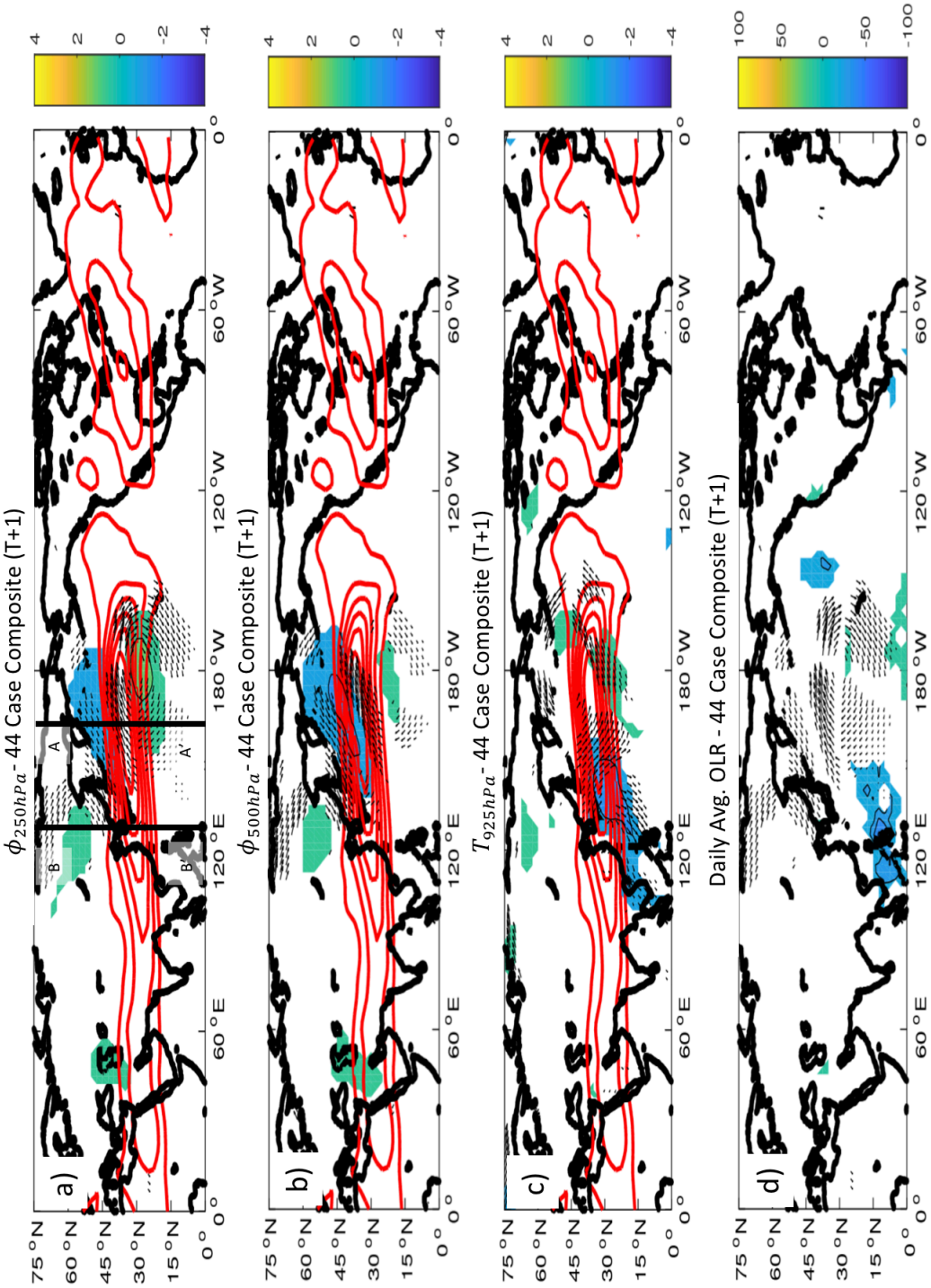

FIG. 4. Same as Fig. 3 but 1 day after composite west Pacific jet superposition (i.e., time T+1). Note that the domain has been expanded to show all longitudes within the Northern Hemisphere.

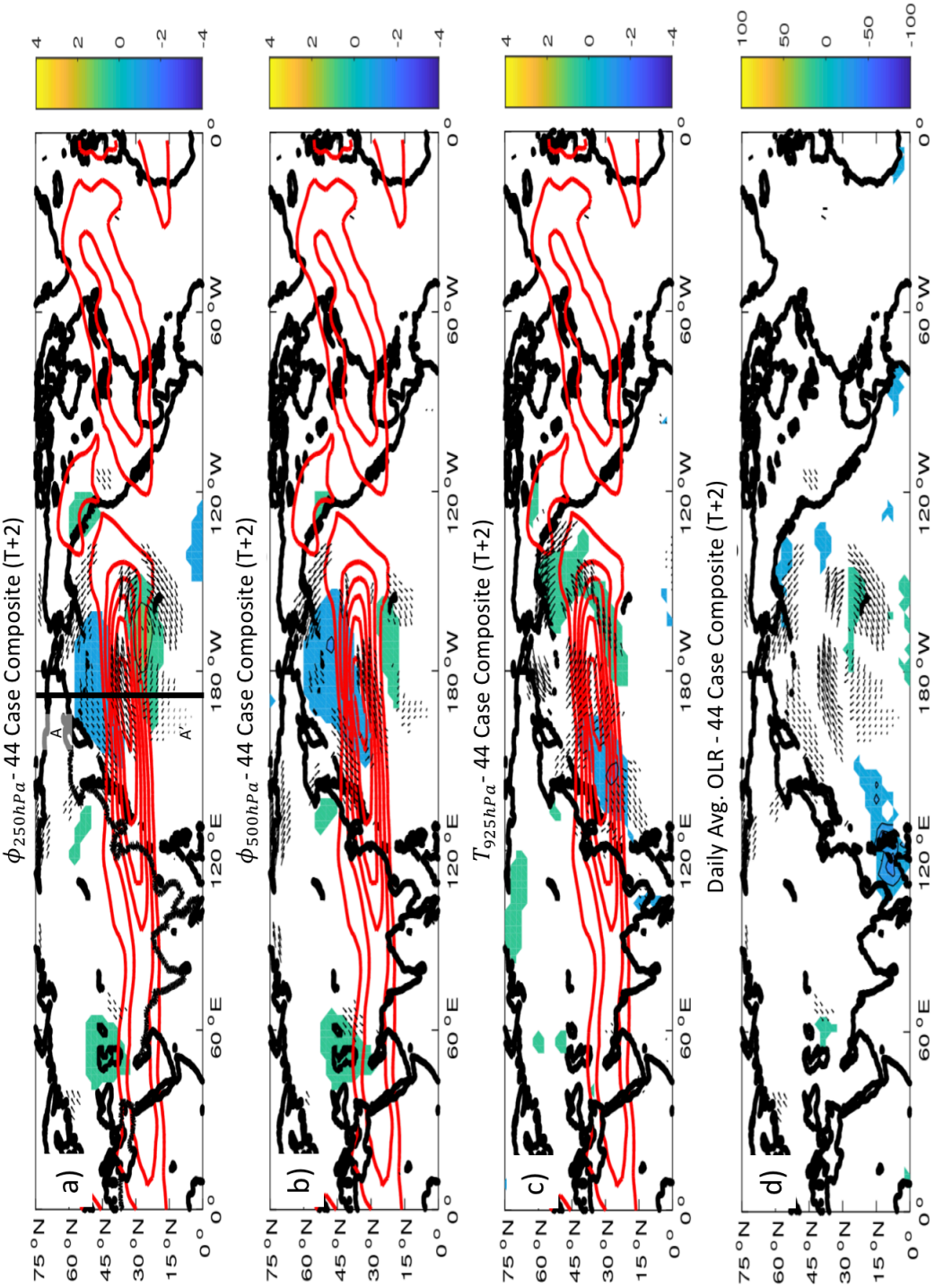

FIG. 5. Same as Fig. 4 but 2 days after composite west Pacific jet superposition (i.e., time T+2).

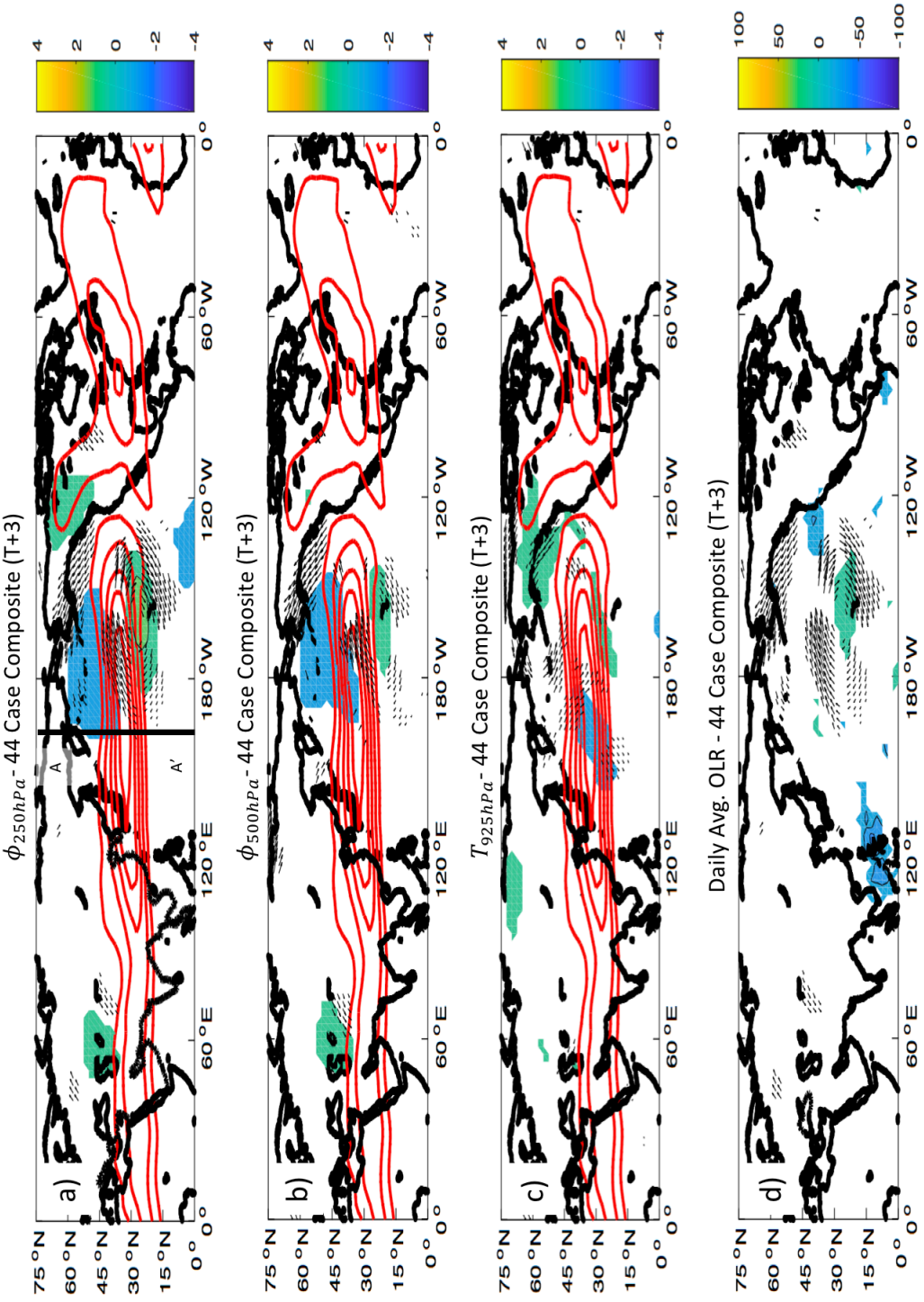

FIG. 6. Same as Fig. 4 but 3 days after composite west Pacific jet superposition (i.e., time T+3).

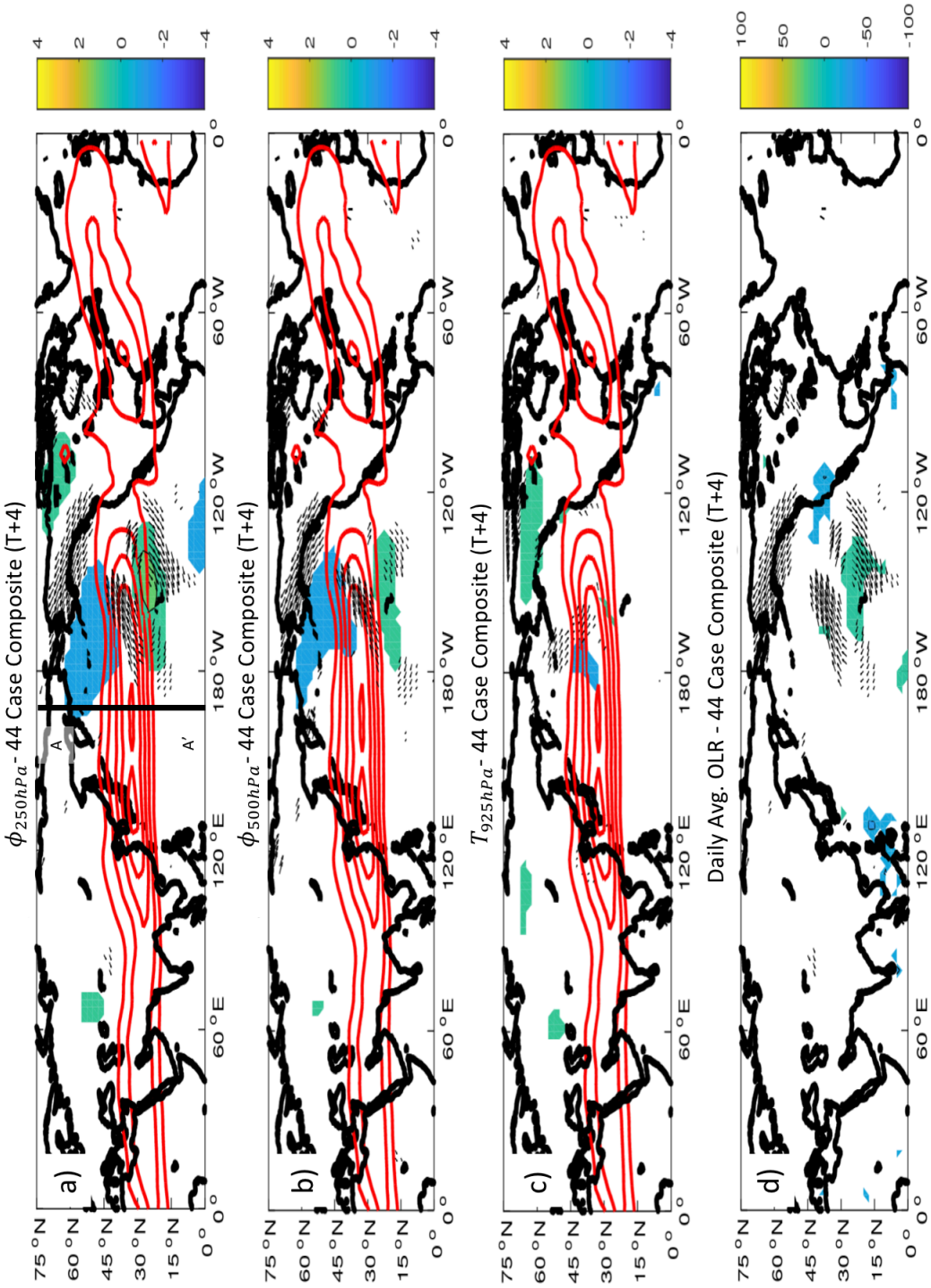

FIG. 7. Same as Fig. 4 but 4 days after composite west Pacific jet superposition (i.e., time T+4).

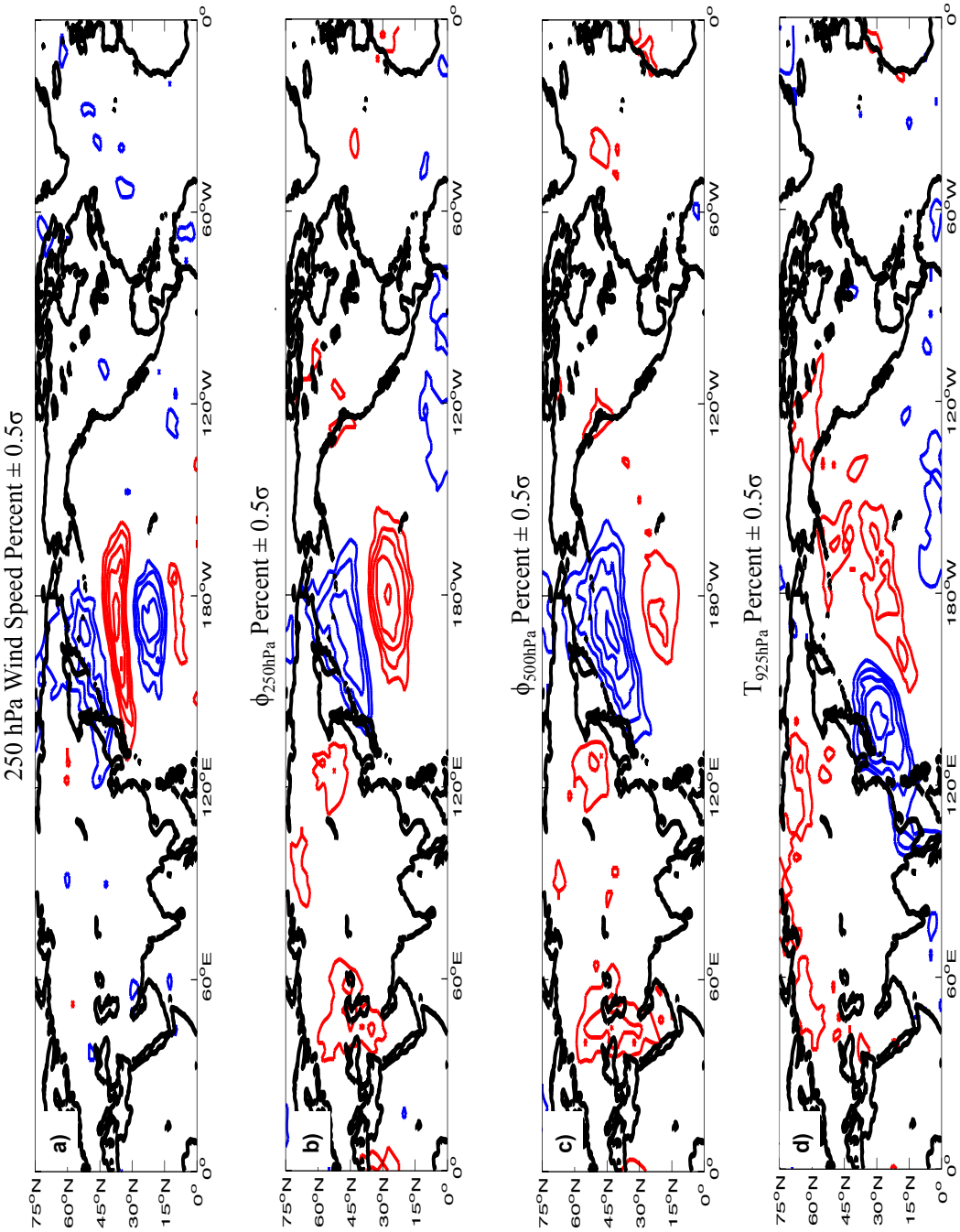

FIG. 8. Percent occurrence of standardized anomalous a) 250 hPa wind speed, b) ϕ_{250}, c) ϕ_{500} and d) T_{925} for all 44 cases used in the composite 1 day after composite west Pacific vertical jet superposition (time T+1). Red (blue) contours indicate regions where the variable of interest with standardized value $\geq 0.5\sigma$ ($\leq$ -0.5σ) occurs in at least 50% of cases contoured every 10%.

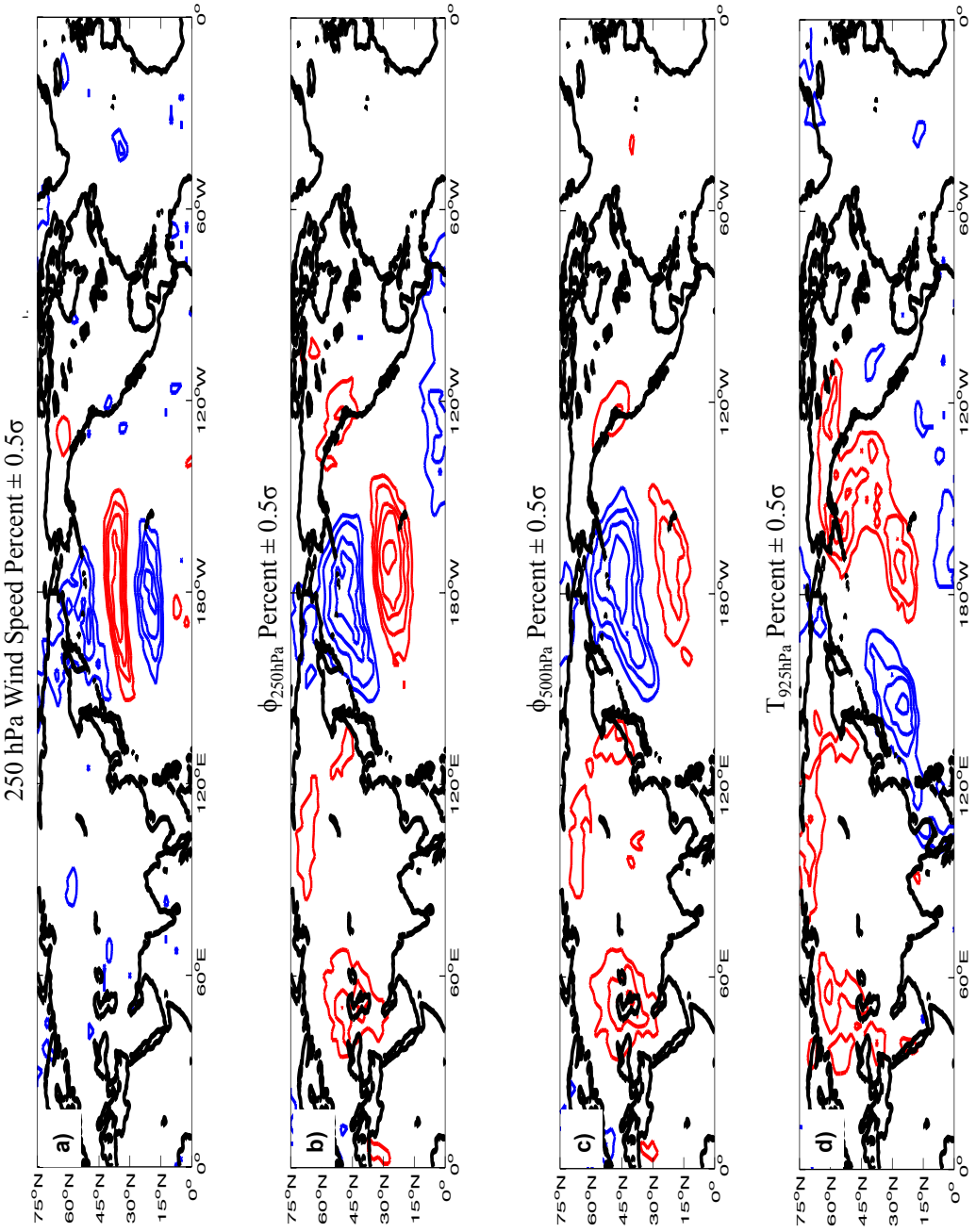

FIG. 9. Same as Fig. 8 but 2 days after composite west Pacific jet superposition (i.e., time T+2).

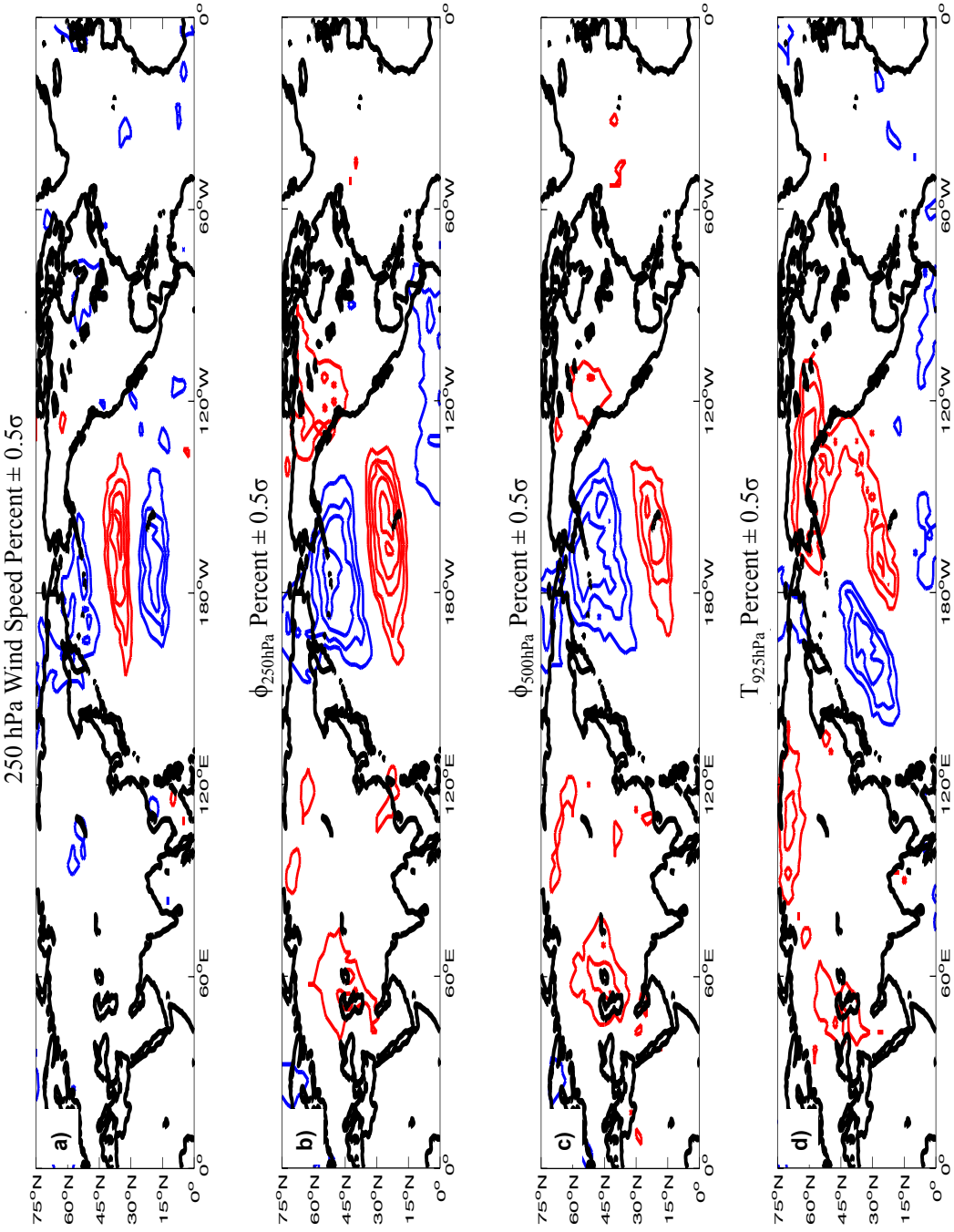

FIG. 10. Same as Fig. 8 but 3 days after composite west Pacific jet superposition (i.e., time T+3).

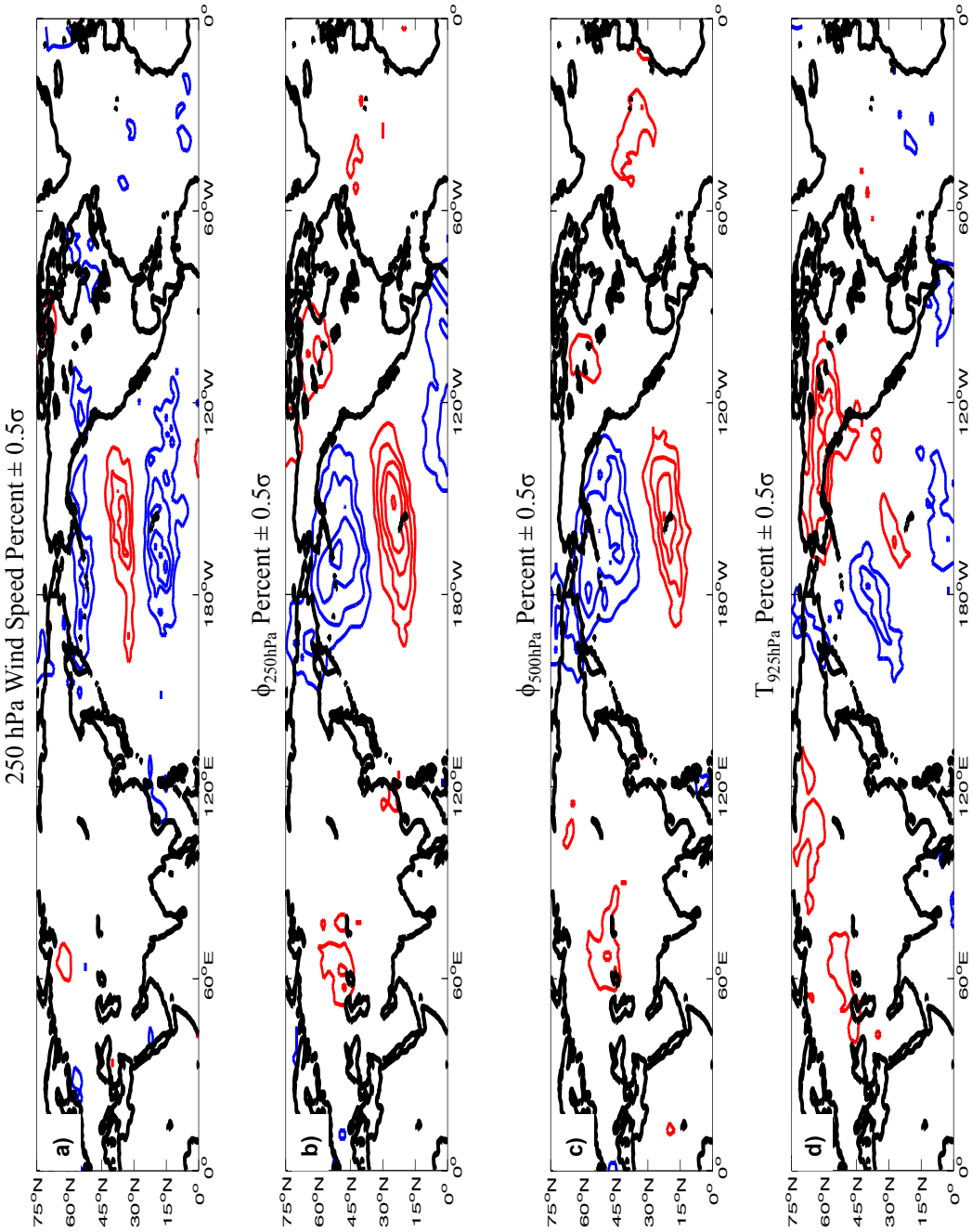

FIG. 11. Same as Fig. 8 but 4 days after composite west Pacific jet superposition (i.e., time T+4).

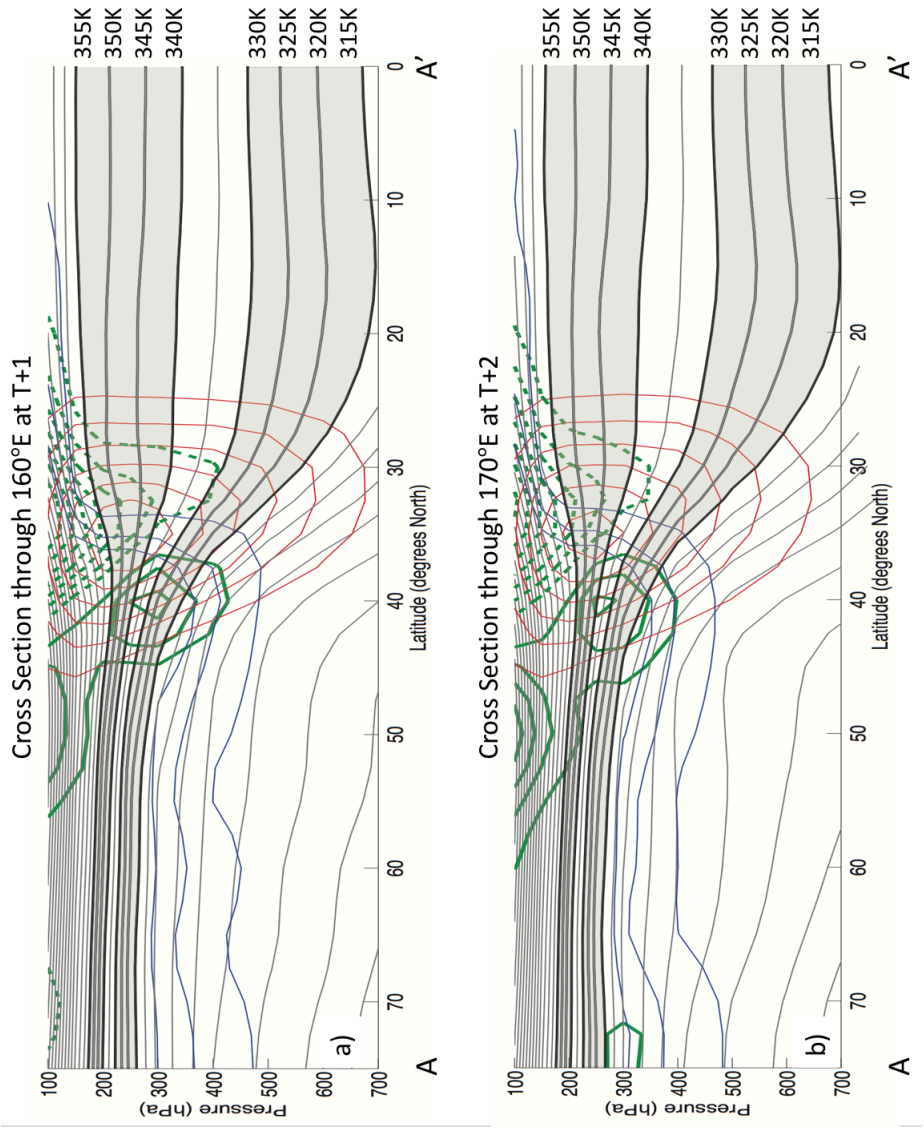

FIG. 12. Composite cross sections through the core of the composite vertically superposed jet in the west Pacific. Each cross section shows wind speed (solid red contour; 10 m s^{-1} intervals starting at 30 m s^{-1}), isentropic surfaces (solid gray contour every 5 K starting at 280 K, with levels within 315-330- and 340-355-K layers in thicker black contour, labeled and shaded in light gray), the 1-3-PVU channel in the upper troposphere (solid blue contour; PVU) and anomalous Ertel PV [solid (dashed) green contour every 0.5 PVU starting at +0.5 (-0.5) PVU]. The cross section locations and times are as follows: a) along 160°E at time T+1 and b) along 170°E at time T+2. Each cross-section is marked on panel a) of Figs. 4-5 (A-A' lines).

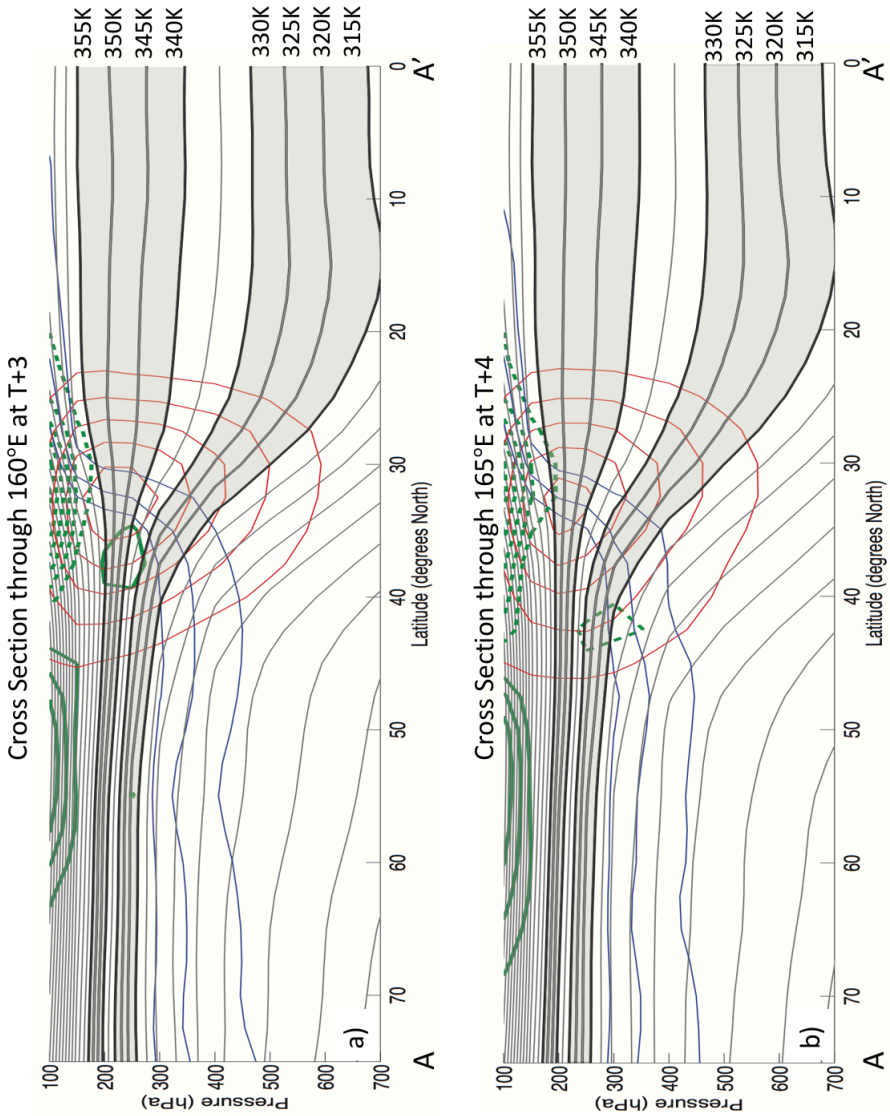

FIG. 13. Same as Fig. 12 except for cross sections a) along 160°E at time T+3 and b) along 165°E at time T+4. Each cross-section is marked on panel a) of Figs. 6-7 (A-A' lines).

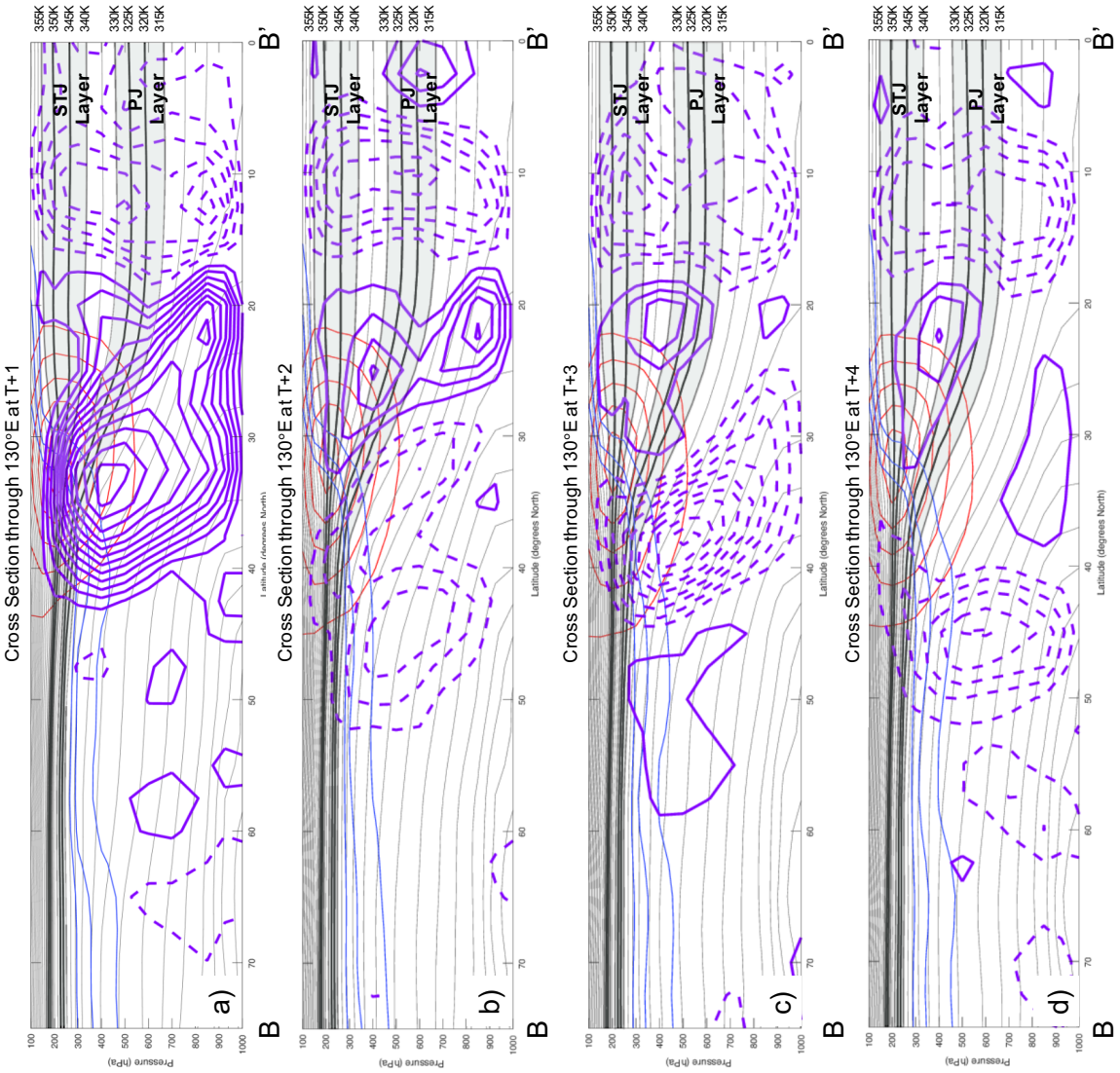

FIG. 14. Composite cross sections taken along 130°E longitude. All conventions are the same as Figs. 12 and 13, but the purple solid (dashed) contours represent anomalous downward (upward) vertical motion every 0.01 Pa s^{-1} starting at +0.01 (-0.01) Pa s^{-1}.

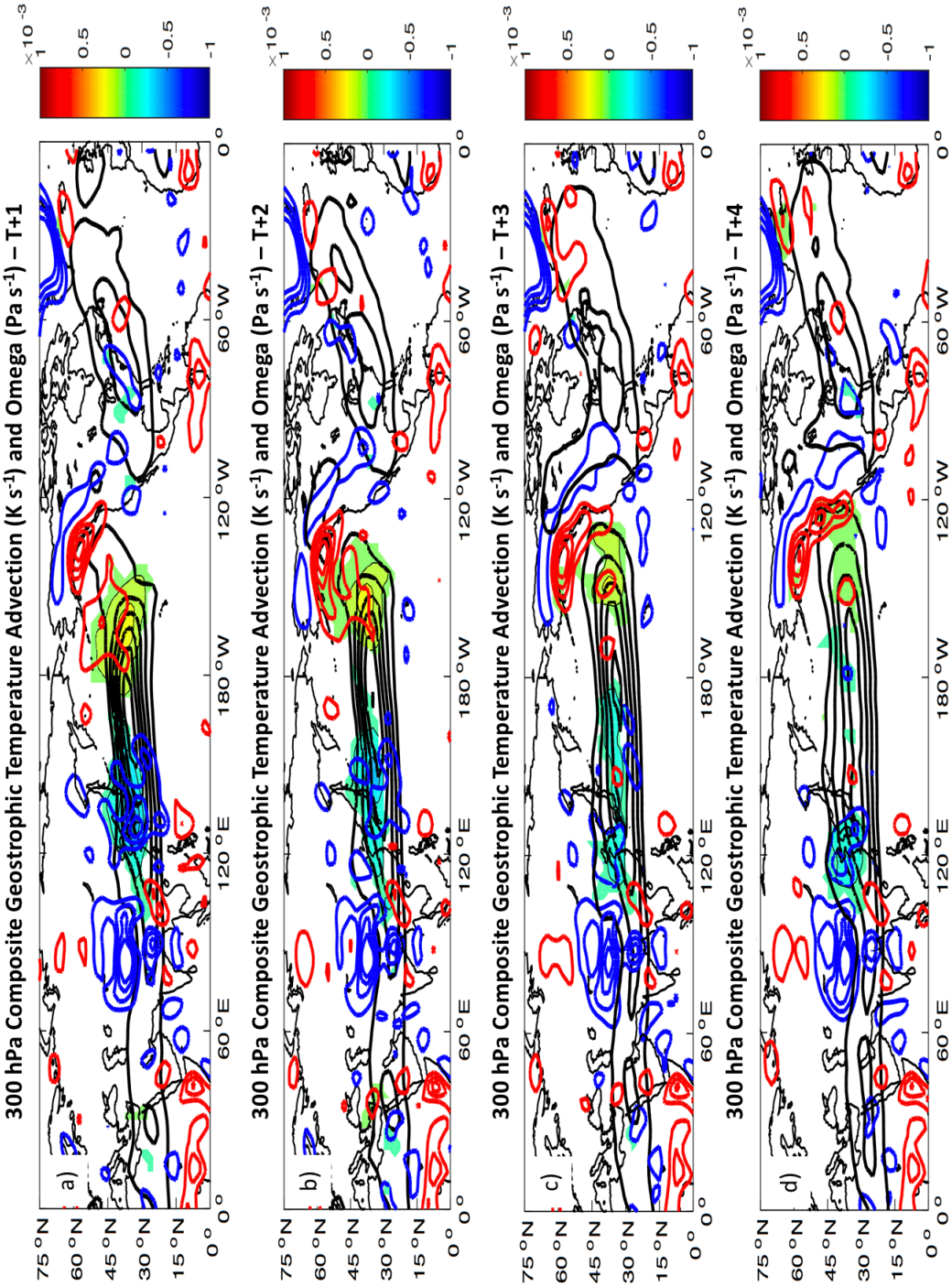

FIG. 15. 300-hPa composite geostrophic temperature advection (fill pattern; K s^{-1}) and vertical motion [red (blue) contour indicates upward (downward) vertical motion] contoured every 0.05 Pa s^{-1} starting at $\pm$ 0.05 Pa s^{-1} for times (a) T+1, (b) T+2, (c) T+3 and (d) T+4. Also plotted on all panels is the 300-hPa composite wind speed (black solid contour) every 10 m s^{-1} starting at 30 m s^{-1}.

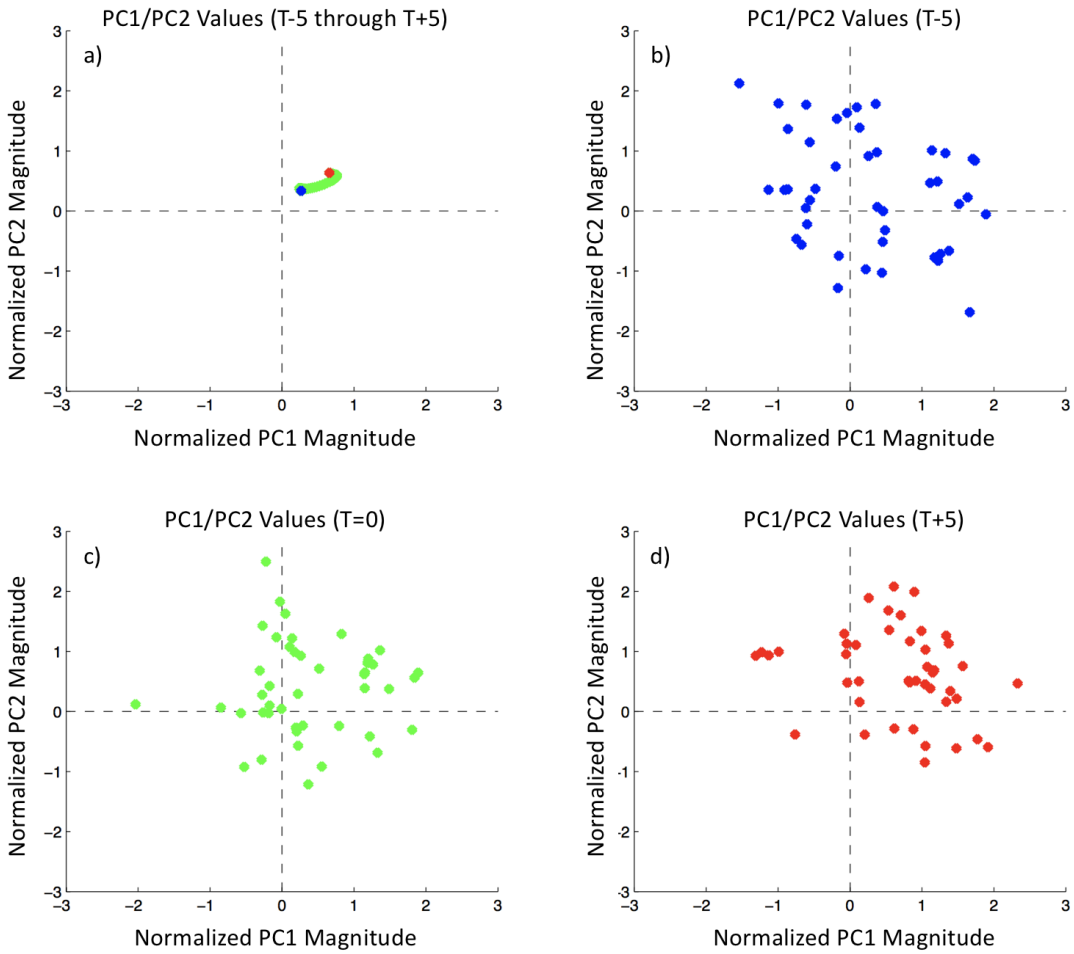

FIG. 16. a) Phase space diagram showing values of normalized principal component (PC) modes 1 (i.e., jet extension/retraction) and 2 (i.e., poleward/equatorward shift) for all 44 west Pacific vertical jet superposition cases (each case shown as solid black line) and the composite event (solid green line) starting at time T-5 (blue dot) and ending at time T+5 (red dot). Each individual day within this time range is marked with a black "X" symbol. b) PC1/PC2 values for all 44 cases at time T-5. c) Same as panel b but for time T=0. d) Same as panel c but for time T+5. See text for further details.

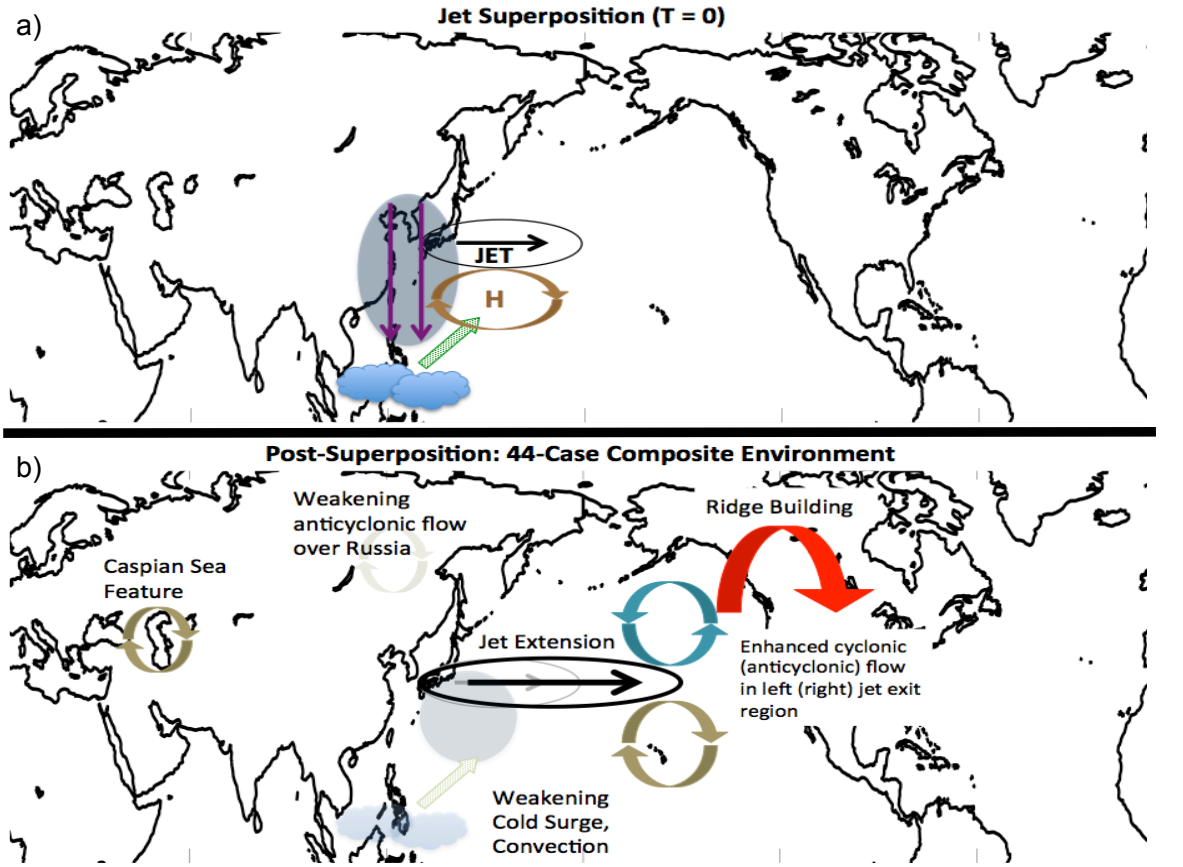

FIG. 17. Conceptual model highlighting evolution of the west Pacific jet and associated large-scale environments after time of west Pacific vertical jet superposition occurrence. a) Key large-scale components associated with west Pacific jet superposition (same conventions as that of Fig. 17 from Handlos and Martin 2016) at time T=0. b) Same as panel a) but 1-4 days after superposition occurrence. The features shown in this panel are those that occur within the majority of cases within the 44-case composite. The jet extension that occurs during this timeframe is shown as a black solid contour with a black vector; the jet at time T=0 is shown in light gray contour with a gray vector. The cyclonic (anticyclonic) circulation in teal (gold) represents the anomalous negative (positive) ϕ within the left (right) jet exit region that propogates eastward as the west Pacific jet extends. The red arrow over northwestern Canada represents the ridge that develops associated with anomalous positive ϕ at 250 and 500 hPa. This ridge develops as the jet extends eastward along with the anomalous cyclonic (anticyclonic) feature in the left (right) jet exit region. Finally, features that were significant in the 44-case composite environment at time T=0 but have weakened at times T+1 through T+4 are faded, including the weakening of the northerly cold surge event, anomalous convection over Indonesia and anticyclonic flow over northern Russia.